Electronic Supplementary Material (ESI) for Dalton Transactions.

Supplementary Information

Molecularly Dispersed Nickel Complexes on N-doped Graphene for Electrochemical CO_2 Reduction

Methasit Juthathan, Teera Chantarojsiri, Kittipong Chainok, Teera Butburee, Patchanita Thamyongkit, Thawatchai Tuntulani, and Pannee Leeladee*

[a] Methasit Juthathan, Prof. Dr. Patchanita Thamyongkit, Prof. Dr. Thawatchai Tuntulani, Assist. Prof. Dr. Pannee Leeladee
Department of Chemistry, Faculty of Science
Chulalongkorn University
Bangkok, Thailand.
E-mail: pannee.l@chula.ac.th

[b] Assist. Prof. Dr. Teera Chantarojsiri
Centre of Excellence for Innovation in Chemistry (PERCH-CIC), Department of Chemistry, Faculty of Science
Mahidol University
Bangkok, Thailand.

[c] Assoc. Prof. Dr. Kittipong Chainok
Thammasat University Research Unit in Multifunctional Crystalline Materials and Applications (TU-McMa), Faculty of Science and Technology
Thammasat University
Pathum Thani, Thailand.

[d] Dr. Teera Butburee
National Nanotechnology Center, National Science and Technology Development Agency, Thailand Science Park
Pathum Thani, Thailand.

Table of Contents

Synthetic Procedures

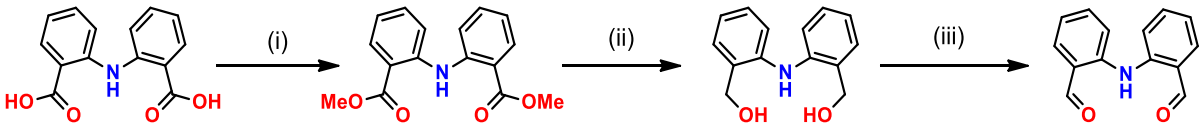

Scheme 1 Synthetic routes of 2,2´-iminobisbenzaldehyde. (i) conc. H_2SO_4, MeOH. (ii) $LiAlH_4$, Et_2O. (iii) MnO_2, Et_2O.

Step i : Synthesis of 2,2´-iminobis(methyl benzoate)

A two-neck round-bottom flask was charged with 2,2´-iminodibenzoic acid (500 mg, 1.94 mmol) and methanol (20 mL), then concentrated H_2SO_4 (1 mL) was slowly added into. The reaction mixture was refluxed for 5 hours and monitored by thin layer chromatography using 1:4 EtOAC: Hexane as a solvent system. After removal of methanol, the reaction was then cautiously added 10 mL of Na_2CO_3 (2.40 g). (Note: the CO_2 bubbling occurs upon the addition of Na_2CO_3). After the bubbling subsides, the solution was extracted with 5 mL of 15% NaCl, followed by CH_2Cl_2 (3 x 10 mL). The combined organic layer was then washed with 10 mL of saturated NaCl, after which the CH_2Cl_2 was removed by reduced pressure to afford the pale-yellow solid as the desired product (477 mg, 86%). ^{1}H NMR (400 MHz, $CDCl_3$, 298 K): δ(ppm) = 3.94 (s, 6H, C*H*$_3$), 6.90 (t, *J* = 7.5 Hz, 2H, Ar*H*), 7.37 (t, *J* = 7.3 Hz, 2H, Ar*H*), 7.55 (d, *J* = 8.5 Hz, 2H, Ar*H*), 7.99 (d, *J* = 6.9 Hz, 2H, Ar*H*), 11.05 (s, 1H, N*H*).

Step ii : Synthesis of 2,2´-iminobis(hydroxymethyl benzene)

To a suspension of $LiAlH_4$ (151 mg, 3.97 mmol) in anhydrous Et_2O (40 mL) was cautiously added 2,2´-iminobis(methyl benzoate) (453 mg, 1.59 mmol) over a 15 minute period. The resulting mixture was stirred overnight, after which was quenched sequentially in ice bath by ethyl acetate (3 mL), water (3 mL), NaOH (3 mL, 15%) and water (20 mL), and then filtered. The precipitate was extracted with boiling chloroform (3 x 10 mL). The solvent was removed under reduced pressure, resulting the crude off-white solid which was then purified by precipitating in CH_2Cl_2/Hexane to afford the white solid (255 mg, 70%). ^{1}H NMR (400 MHz, DMSO-d_6, 298 K): δ(ppm) = 4.48 (d, *J* = 5.0 Hz, 4H, C*H*$_2$), 5.26 (t, *J* = 5.1 Hz, 2H, O*H*), 6.87 (t, *J* = 7.2 Hz, 2H, Ar*H*), 7.04 (d, *J* = 7.9 Hz, 2H, Ar*H*), 7.15 (t, *J* = 7.4 Hz, 2H, Ar*H*), 7.31 (d, *J* = 7.3 Hz, 2H, Ar*H*), 7.40 (s, 1H, N*H*).

Step iii: Synthesis of 2,2´-iminobisbenzaldehyde

To a colourless solution of 2,2´-iminobis(hydroxymethyl benzene) (230 mg, 1.00 mmol) in dry Et_2O (30 mL) was added an activated MnO_2 (1.75 g, 20.13 mmol). The resulting black suspension was stirred at room temperature overnight. The MnO_2 was then filtered off and extracted with boiling chloroform (3 x 10 mL). The combined extracts and filtrate were concentrated to yield a yellow solid. This crude yellow solid was purified by chromatography on silica gel with 1:4 EtOAc: Hexane (R_f = 0.4), giving the title product as a bright yellow crystalline solid (138 mg, 62%). ^{1}H NMR (400 MHz, $CDCl_3$, 298 K): δ(ppm) = 7.08 (t, *J* = 7.3 Hz, 2H, Ar*H*), 7.47 (t, *J* = 7.6 Hz, 2H, Ar*H*), 7.55 (d, *J* = 8.0 Hz, Ar*H*), 7.71 (d, *J* = 7.7 Hz, 2H, Ar*H*), 10.03 (s, 2H, C*H*O), 11.36 (s, 1H, N*H*).

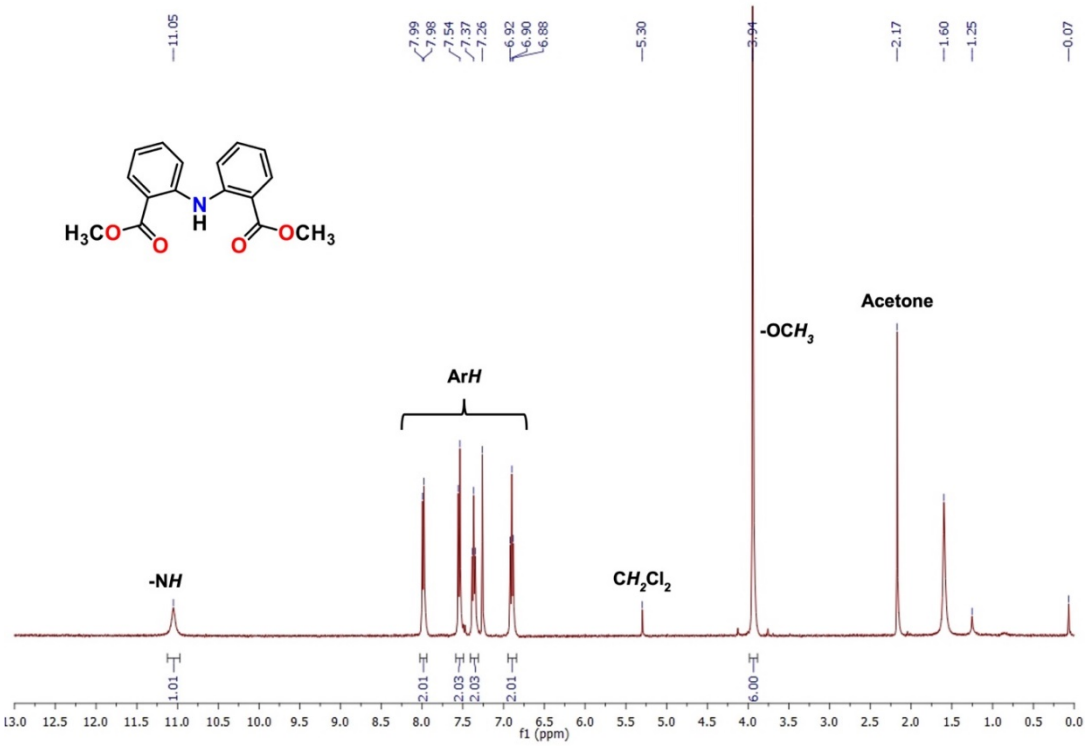

Fig. S1 ^{1}H NMR spectrum of 2,2´-iminobis(methyl benzoate) in $CDCl_3$.

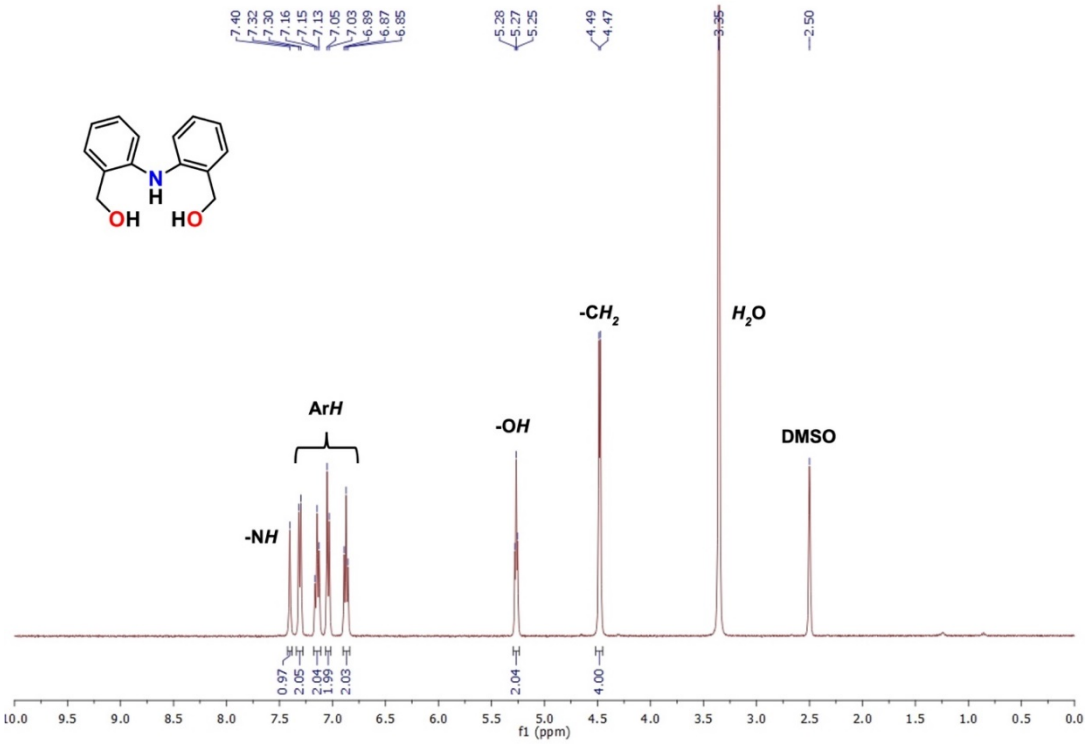

Fig. S2 ^{1}H NMR spectrum of 2,2´-iminobis(hydroxymethyl benzene) in DMSO-d_6.

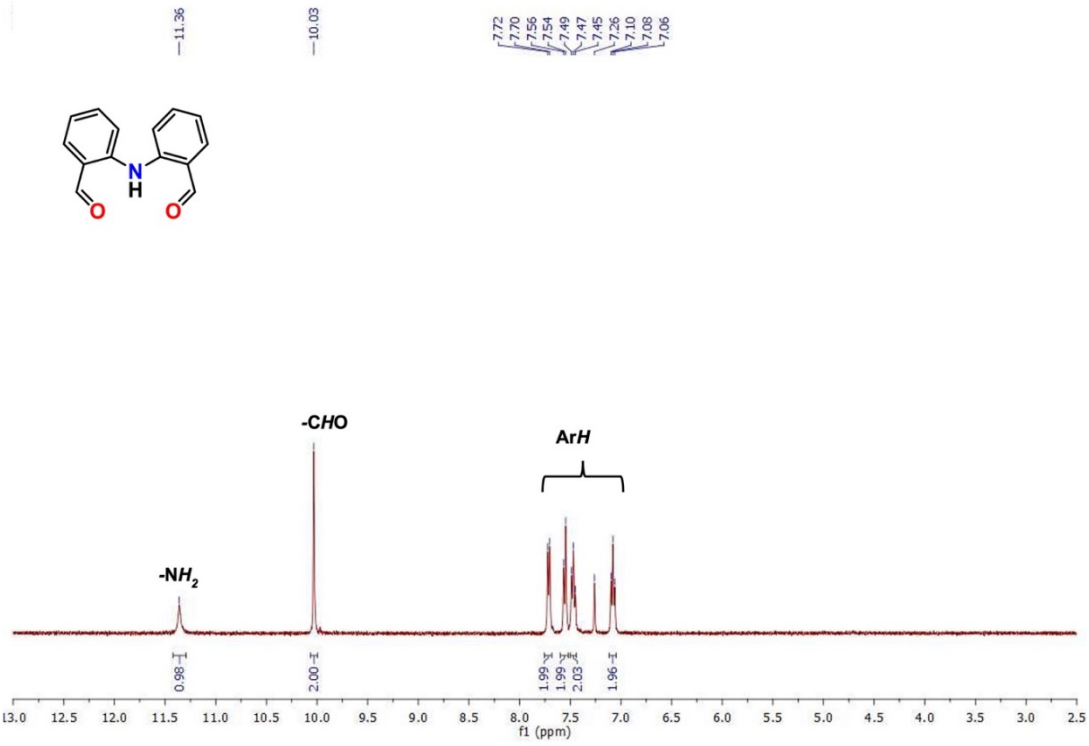

Fig. S3 ^{1}H NMR spectrum of 2,2´-iminobisbenzaldehyde in $CDCl_3$.

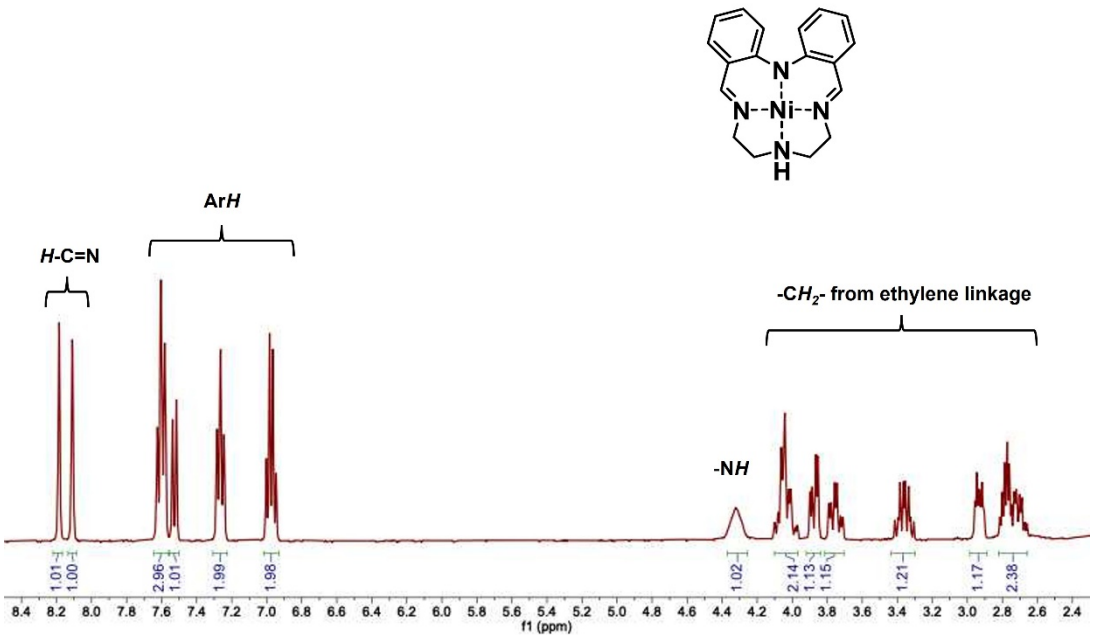

Fig. S4 ^{1}H NMR spectrum of [1-Ni](BF$_4$) in CD$_3$CN.

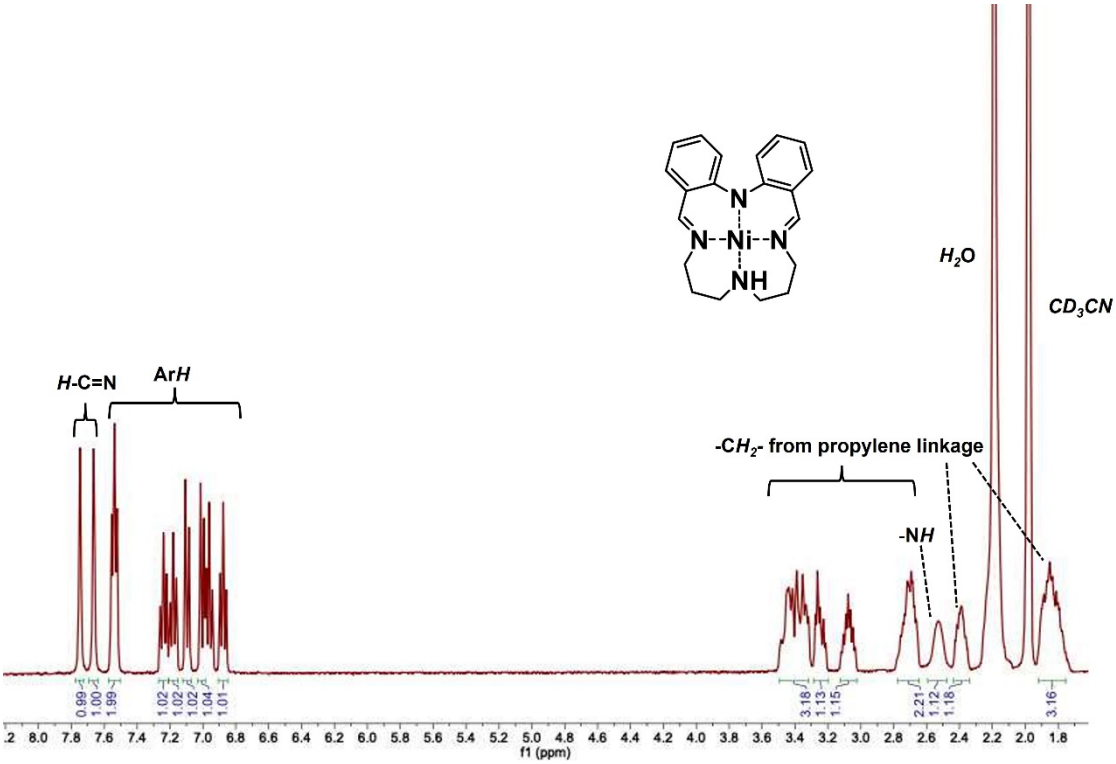

Fig. S5 ^{1}H NMR spectrum of [2-Ni](BF$_4$) in CD$_3$CN.

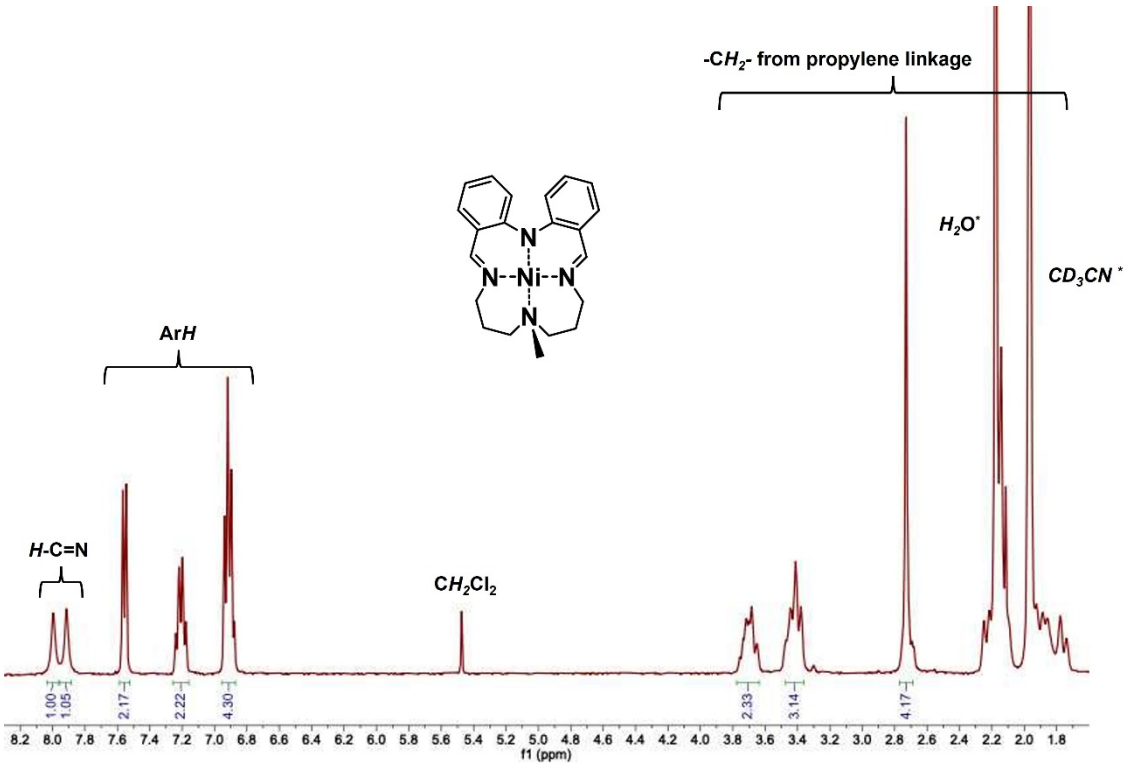

Fig. S6 ^{1}H NMR spectrum of [2-Ni]^{Me}(BF_4) in CD_3CN.

* some *H* peaks from propylene linkage overlap with the peaks of solvent.

Mass Spectrum List Report

Analysis Info

Analysis Name	D:\Data\Data Service\191111\PLMJ046_RA2_01_3478.d	Acquisition Date	11/11/2019 5:40:19 PM
Method	nv_pos_6min_profile_wguardcol_50-1500_191021.m	Operator	CU.
Sample Name	PLMJ046	Instrument / Ser#	micrOTOF-Q II 10335
Comment			

Acquisition Parameter

Source Type	ESI	Ion Polarity	Positive	Set Nebulizer	3.0 Bar
Focus	Not active	Set Capillary	4000 V	Set Dry Heater	200 °C
Scan Begin	50 m/z	Set End Plate Offset	-500 V	Set Dry Gas	8.0 l/min
Scan End	1500 m/z	Set Collision Cell RF	250.0 Vpp	Set Divert Valve	Waste

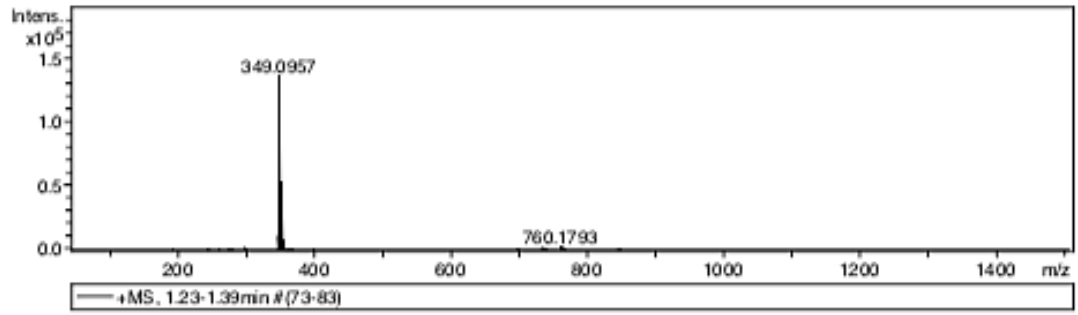

#	m/z	Res.	S/N	I	FWHM
1	192.9438	7767	462.7	268	0.0248
2	243.9411	8473	243.6	331	0.0288
3	260.9312	9109	164.3	266	0.0286
4	277.9221	9014	159.6	300	0.0308
5	298.2739	9393	575.6	1691	0.0318
6	299.2777	9350	108.3	328	0.0320
7	346.0726	9988	52.9	382	0.0346
8	347.0796	9845	1530.1	11148	0.0353
9	348.0841	9542	541.7	3996	0.0365
10	349.0957	8750	18229.6	136074	0.0399
11	350.0978	9409	3647.1	27551	0.0372
12	351.0918	9184	6875.1	52542	0.0382
13	352.0935	9649	1629.0	12596	0.0365
14	353.0898	9541	994.4	7778	0.0370
15	354.0919	9889	202.3	1601	0.0358
16	355.0883	9793	225.7	1806	0.0363
17	356.0916	9698	50.2	407	0.0367
18	365.0898	9639	54.2	484	0.0379
19	367.0956	8069	29.7	271	0.0455
20	733.1599	13351	262.8	1000	0.0549
21	734.1652	12836	103.0	395	0.0572
22	735.1579	13189	296.9	1141	0.0557
23	736.1586	13309	125.5	485	0.0553
24	737.1551	12689	141.6	550	0.0581
25	760.1793	12433	599.0	2570	0.0611
26	761.1810	12693	258.6	1115	0.0600
27	762.1769	12301	516.7	2236	0.0620
28	763.1775	12622	228.6	994	0.0605
29	764.1730	12718	191.6	837	0.0601
30	765.1746	13720	89.2	392	0.0558

Fig. S7 High resolution mass spectrum of [1-Ni](BF_4)

Mass Spectrum List Report

Analysis Info

Analysis Name	D:\Data\Data Service\191125\PLMJ048_RA3_01_3483.d	Acquisition Date	11/25/2019 4:38:16 PM
Method	nv_pos_6min_profile_wguardcol_50-1500_191021.m	Operator	CU.
Sample Name	PLMJ048	Instrument / Ser#	micrOTOF-Q II 10335
Comment			

Acquisition Parameter

Source Type	ESI	Ion Polarity	Positive	Set Nebulizer	3.0 Bar
Focus	Not active	Set Capillary	4000 V	Set Dry Heater	200 °C
Scan Begin	50 m/z	Set End Plate Offset	-500 V	Set Dry Gas	8.0 l/min
Scan End	1500 m/z	Set Collision Cell RF	250.0 Vpp	Set Divert Valve	Waste

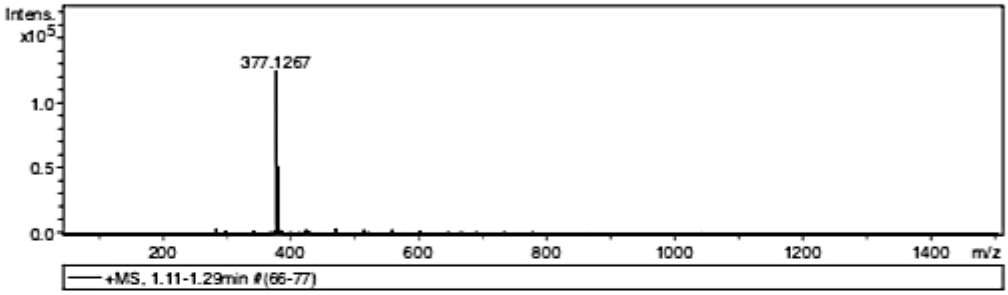

#	m/z	Res.	S/N	I	FWHM
1	284.3304	9040	852.4	3438	0.0315
2	298.2737	9064	326.9	2055	0.0329
3	341.2654	9880	127.5	1952	0.0345
4	368.4245	10305	79.2	1665	0.0358
5	375.1110	10005	78.2	1753	0.0375
6	377.1267	8803	5469.0	124724	0.0428
7	378.1291	9683	1203.0	27691	0.0391
8	379.1223	9651	2205.5	51223	0.0393
9	380.1246	10072	557.9	13078	0.0377
10	381.1209	9948	329.4	7790	0.0383
11	382.1230	10224	68.0	1624	0.0374
12	383.1207	9893	72.8	1754	0.0387
13	384.1873	9507	41.4	1008	0.0404
14	385.2911	10034	76.1	1869	0.0384
15	400.3759	10348	49.2	1087	0.0387
16	422.1108	10717	55.9	1026	0.0394
17	425.3596	10554	185.1	3287	0.0403
18	428.4082	10419	72.2	1247	0.0411
19	429.3166	10410	61.7	1056	0.0412
20	469.3851	10926	379.0	3869	0.0430
21	470.3884	10832	111.7	1122	0.0434
22	513.4115	10772	389.5	3144	0.0477
23	514.4152	11333	126.1	1020	0.0454
24	557.4384	11798	339.0	2818	0.0473
25	601.4650	11701	232.1	1991	0.0514
26	645.4893	12497	192.9	1709	0.0517
27	666.6385	12185	173.8	1564	0.0547
28	689.5151	12424	165.8	1452	0.0555
29	733.5421	12982	183.7	1399	0.0565
30	777.5684	12950	158.6	1036	0.0600

Fig. S8 High resolution mass spectrum of [2-Ni](BF_4)

Mass Spectrum List Report

Analysis Info

Analysis Name	D:\Data\Data Service\201221\PLMJ079_NiN4Me_RC2_01_5092.d	Acquisition Date	12/21/2020 3:44:40 PM
Method	nv_pos_5min_profile_190214.m	Operator	CU.
Sample Name	PLMJ079_NiN4Me	Instrument / Ser#	micrOTOF-Q II 10335
Comment			

Acquisition Parameter

Source Type	ESI	Ion Polarity	Positive	Set Nebulizer	3.0 Bar
Focus	Not active	Set Capillary	4000 V	Set Dry Heater	200 °C
Scan Begin	100 m/z	Set End Plate Offset	-500 V	Set Dry Gas	8.0 l/min
Scan End	1500 m/z	Set Collision Cell RF	250.0 Vpp	Set Divert Valve	Waste

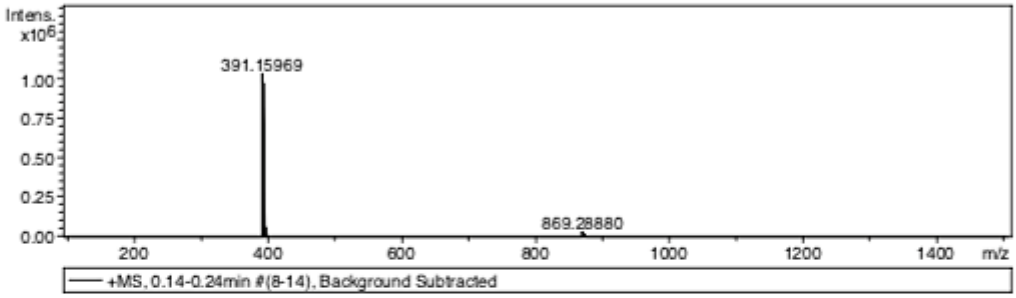

#	m/z	Res.	S/N	I	FWHM
1	195.57037	6894	167.9	1722	0.02837
2	196.07397	6746	329.1	3363	0.02907
3	196.57268	6441	142.5	1459	0.03052
4	197.07094	6859	141.9	1451	0.02873
5	391.15969	3156	196.8	1033315	0.12395
6	392.14840	6414	155.1	827626	0.06114
7	393.14618	4835	179.7	973995	0.08131
8	394.14117	8152	86.0	473290	0.04835
9	395.13697	8588	51.1	285388	0.04601
10	397.13349	9506	10.3	59077	0.04178
11	868.29041	11016	11.8	8178	0.07882
12	869.28880	10413	49.5	34623	0.08348
13	870.28925	10866	32.4	22957	0.08009
14	871.28523	10567	44.2	31777	0.08245
15	872.28516	10800	22.4	16296	0.08076
16	873.28234	10732	16.3	12062	0.08137
17	1349.43196	11821	25.5	1120	0.11415

Fig. S9 High resolution mass spectrum of $[2\text{-Ni}]^{Me}(BF_4)$.

Electrochemical Studies in Non-aqueous Electrolyte

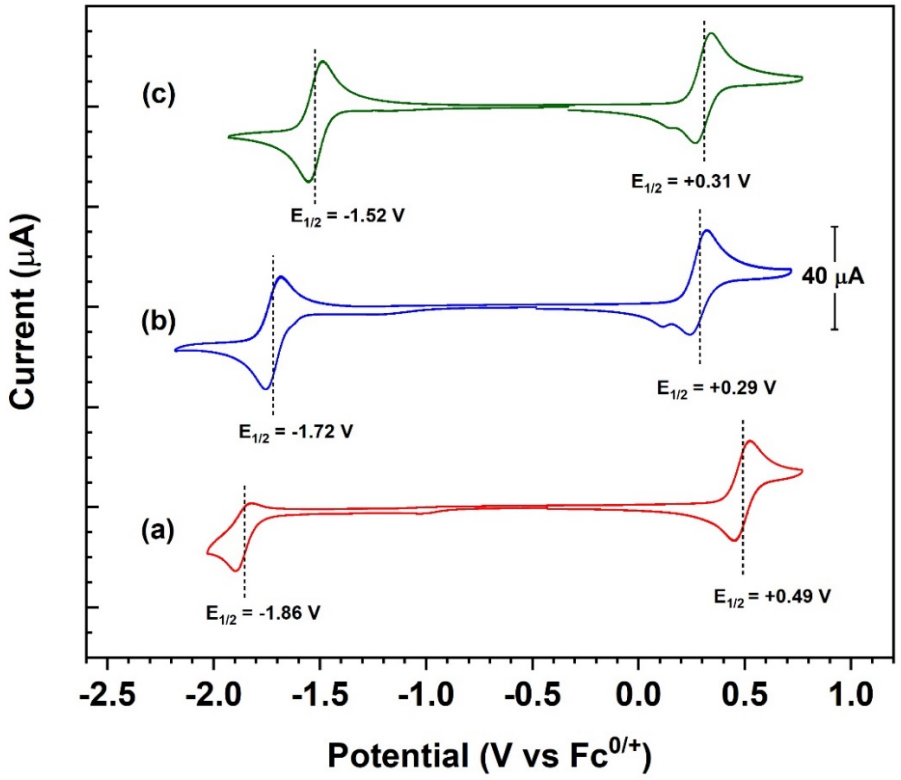

Fig. S10 CVs of 1 mM **(a) 1-Ni**, **(b) 2-Ni** and **(c) [2-Ni]^{Me}** recorded in N_2-saturated CH_3CN/ 0.1 M Bu_4NPF_6 solution (v = 0.1 V/s, glassy carbon electrode).

Table S1 Electrochemical data of Schiff base nickel macrocycles. [a]

Complex	E_{pc1} (V)	E_{pa1} (V)	$E_{1/2}$ (V)[b] [ΔE_p (mV)][c]	E_{pc2} (V)	E_{pa2} (V)	$E_{1/2}$ (V)[b] [ΔE_p (mV)][c]
1-Ni	+0.45	+0.52	+0.49 [73]	-1.89	-1.82	-1.86 [80]
2-Ni	+0.25	+0.33	+0.29 [82]	-1.75	-1.68	-1.72 [71]
[2-Ni]^{Me}	+0.27	+0.34	+0.31 [76]	-1.56	-1.49	-1.52 [66]

[a] All voltammograms were recorded in CH_3CN; the potentials are reported *vs.* the $Fc^{+/0}$ couple. Conditions: scan rate = 100 mV/s, compound (1 mM), Bu_4NPF_6 (0.1 M), glassy carbon working electrode. Under these conditions we found ΔE_p ($Fc^{+/0}$) = 65 mV. [b] $E_{1/2} = (E_{pc} + E_{pa})/ 2$, when E_{pc} = cathodic peak potential and E_{pa} = anodic peak potential. [C] $\Delta E_p = |E_{pc} - E_{pa}|$.

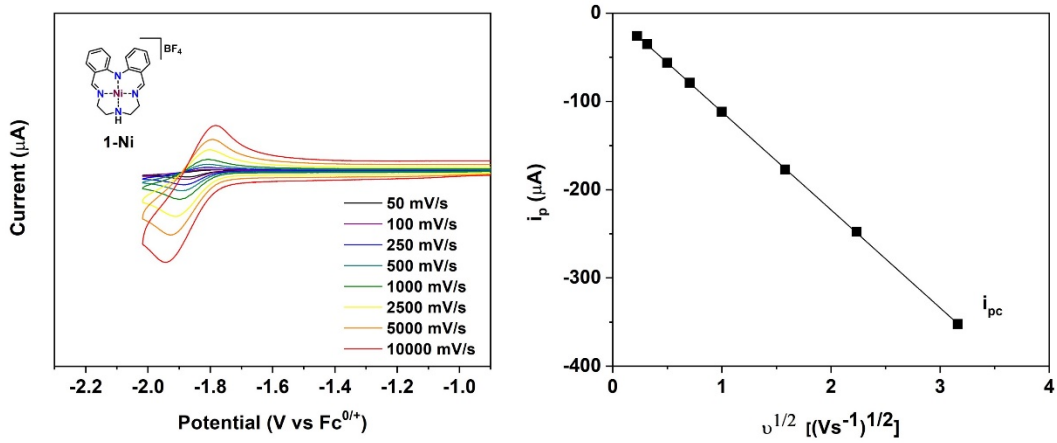

Fig. S11 CVs of **1-Ni** in CH_3CN at different scan rate and plots of reductive current vs. the square root of the scan rate of **1-Ni** in CH_3CN at E = -1.86 V vs. $Fc^{+/0}$.

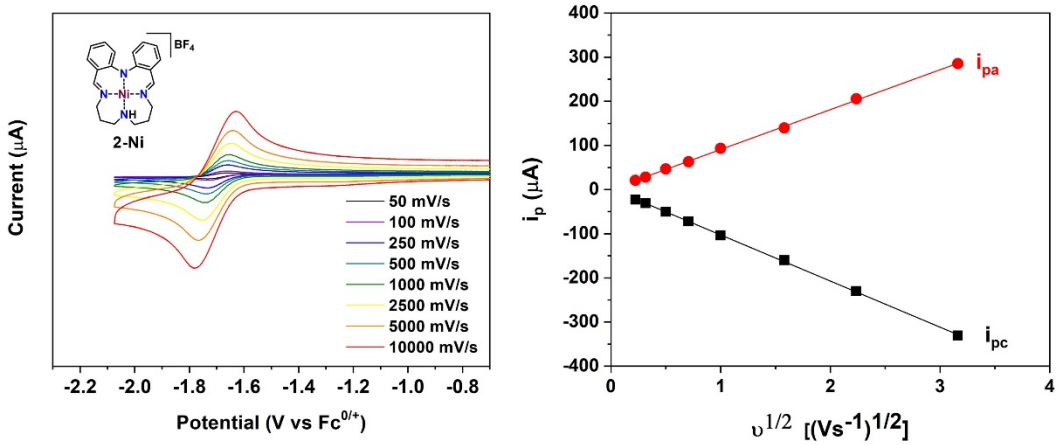

Fig. S12 CVs of **2-Ni** in CH_3CN at different scan rate and plots of reductive and oxidative currents vs. the square root of the scan rate of **2-Ni** in CH_3CN at E = -1.72 V vs. $Fc^{+/0}$.

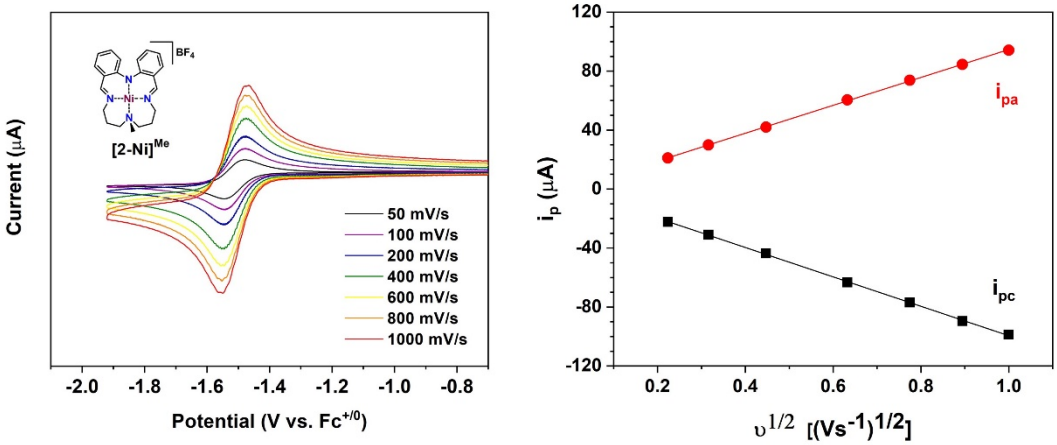

Fig. S13 CVs of **[2-Ni]^{Me}** in CH_3CN at different scan rate and plots of reductive and oxidative currents vs. the square root of the scan rate of **[2-Ni]^{Me}** in CH_3CN at E = -1.52 V vs. $Fc^{+/0}$.

Table S2 Redox potential of Ni^{II}/Ni^{I} couples of **1-Ni** at different scan rates.

Scan rate (V s^{-1})	E_{pc} (V)	E_{pa} (V)	$E_{1/2}$ (V)
0.05	-1.89	-1.82	-1.85
0.1	-1.89	-1.82	-1.85
0.25	-1.90	-1.81	-1.85
0.5	-1.90	-1.81	-1.85
1	-1.92	-1.80	-1.85
2.5	-1.92	-1.79	-1.85
5	-1.92	-1.79	-1.85
10	-1.95	-1.78	-1.86

Table S3 Reductive current of Ni^{II}/Ni^{I} couples of **1-Ni** at different scan rates.

Scan rate (V s^{-1})	i_{pc} (μA)	i_{pa} (μA)	i_{pc}/ i_{pa}
0.05	23.01	-	-
0.1	30.96	-	-
0.25	50.35	-	-
0.5	72.12	-	-
1	104.10	-	-
2.5	160.20	-	-
5	230.50	-	-
10	330.75	-	-

Table S4 Redox potential of Ni^{II}/Ni^{I} couples of **2-Ni** at different scan rates.

Scan rate (V s^{-1})	E_{pc} (V)	E_{pa} (V)	$E_{1/2}$ (V)
0.05	-1.75	-1.68	-1.72
0.1	-1.75	-1.68	-1.72
0.25	-1.75	-1.68	-1.72
0.5	-1.75	-1.68	-1.72
1	-1.76	-1.67	-1.72
2.5	-1.76	-1.66	-1.71
5	-1.77	-1.66	-1.72
10	-1.78	-1.65	-1.72

Table S5 Reductive and oxidative current of Ni^{II}/Ni^{I} couples of **2-Ni** at different scan rates.

Scan rate (V s^{-1})	i_{pc} (μA)	i_{pa} (μA)	i_{pc}/ i_{pa}
0.05	23.01	20.84	1.10
0.1	30.96	28.26	1.10
0.25	50.35	46.62	1.08
0.5	72.12	63.05	1.14
1	104.10	93.20	1.12
2.5	160.20	139.30	1.15
5	230.50	205.80	1.12
10	330.75	285.13	1.16

Table S6 Redox potential of Ni^{II}/Ni^{I} couples of $[\mathbf{2\text{-}Ni}]^{Me}$ at different scan rates.

Scan rate (V s^{-1})	E_{pc} (V)	E_{pa} (V)	$E_{1/2}$ (V)
0.05	-1.55	-1.49	-1.52
0.1	-1.55	-1.49	-1.52
0.2	-1.56	-1.49	-1.53
0.4	-1.56	-1.48	-1.52
0.6	-1.56	-1.48	-1.52
0.8	-1.56	-1.49	-1.53
1.0	-1.56	-1.48	-1.52

Table S7 Reductive and oxidative current of Ni^{II}/Ni^{I} couples of $[\mathbf{2\text{-}Ni}]^{Me}$ at different scan rates.

Scan rate (V s^{-1})	i_{pc} (μA)	i_{pa} (μA)	i_{pc}/ i_{pa}
0.05	22.32	21.12	1.05
0.1	31.01	29.83	1.04
0.2	43.74	42.00	1.04
0.4	63.39	60.45	1.05
0.6	76.92	73.76	1.04
0.8	89.57	84.54	1.06
1.0	98.81	94.22	1.05

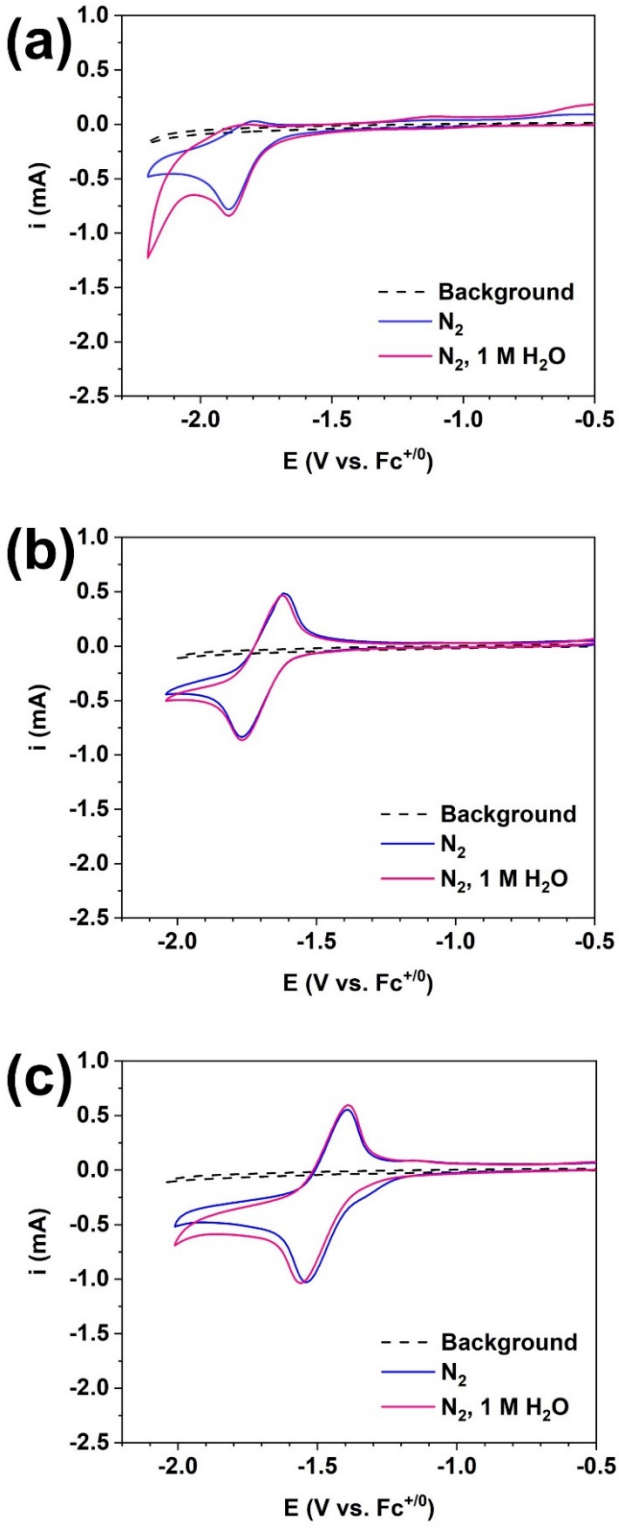

Fig. S14 Cyclic voltammograms of (a) **1-Ni**, (b) **2-Ni**, and (c) **[2-Ni]^{Me}** at 1 mM concentration in 0.1 M NBu_4PF_6/CH_3CN (v = 0.1 V/s) under N_2 (blue) and under N_2 with 1 M H_2O (pink). Background signals were collected under CO_2-saturated 0.1 M NBu_4PF_6/CH_3CN and illustrated in black-dashed line.

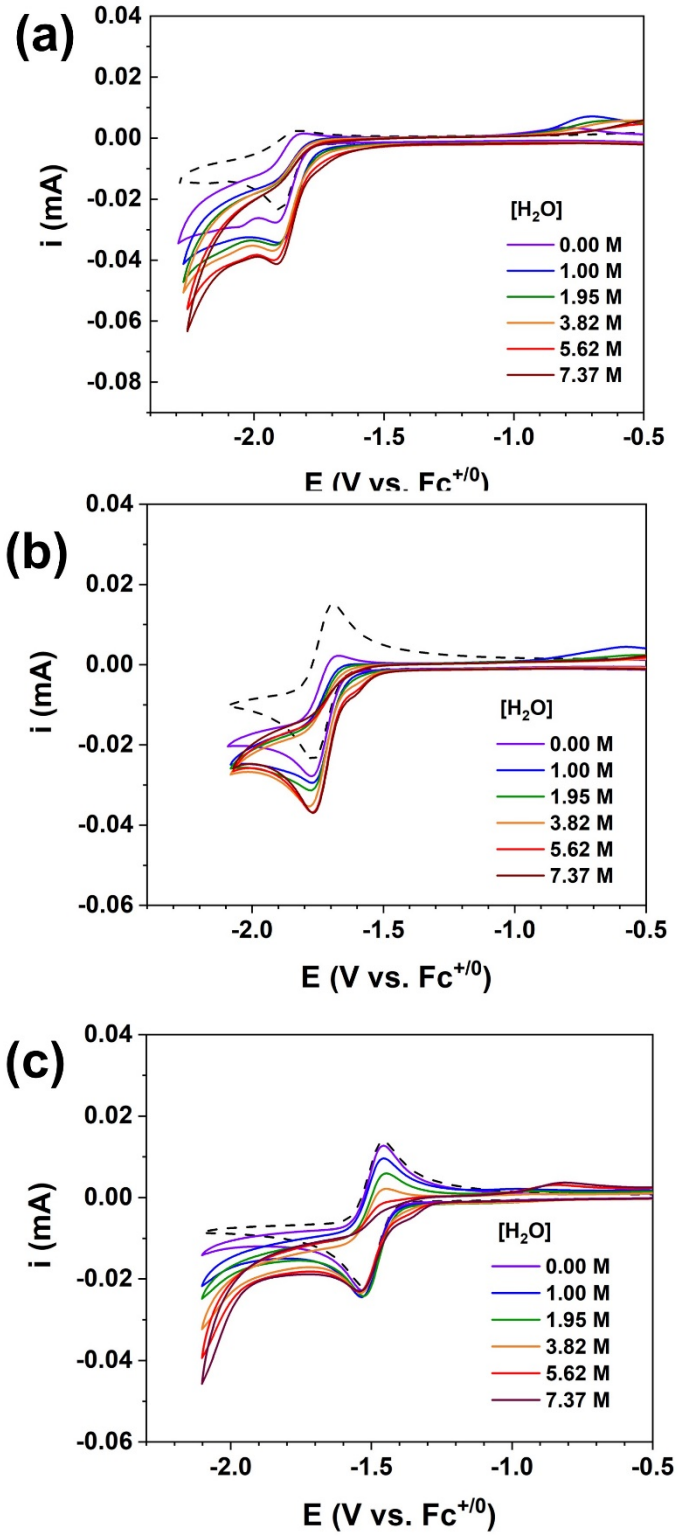

Fig. S15 Cyclic voltammograms (CVs) of (a) 1-Ni, (b) 2-Ni and (c) $[2\text{-Ni}]^{Me}$ in CO_2-saturated CH_3CN/ 0.1 M Bu_4NPF_6 with the various concentration of H_2O. CVs in N_2-saturated CH_3CN/ 0.1 M Bu_4NPF_6 were illustrated in the broken line. Glassy carbon (Area = 0.071 cm^2) was used as a working electrode.

UV-visible Spectra of Ni Complexes Before and After Adsorption on NG

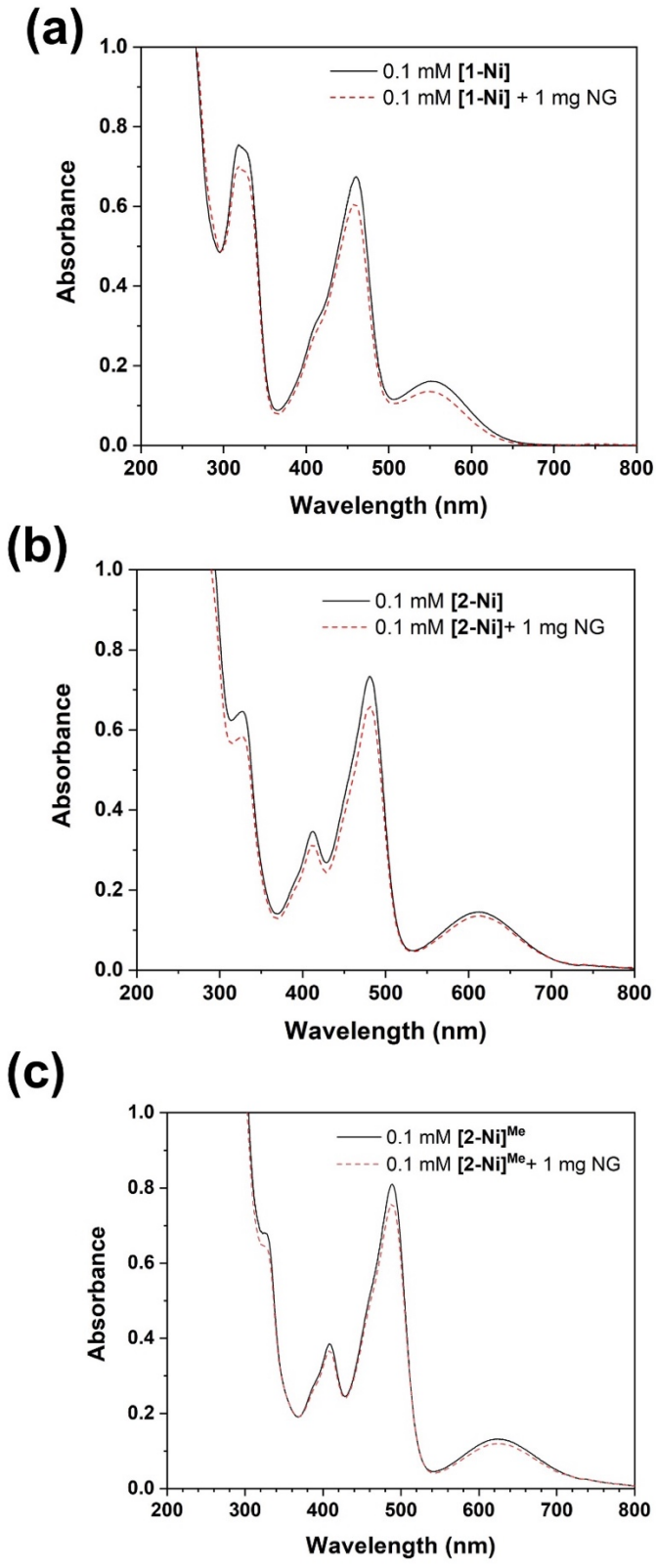

Fig. S16 UV-visible spectra of (a) **1-Ni**, (b) **2-Ni** and (c) **[2-Ni]^{Me}** complexes before (black solid line) and after (red dotted line) adsorption on NG.

Scanning Electron Microscopic Images

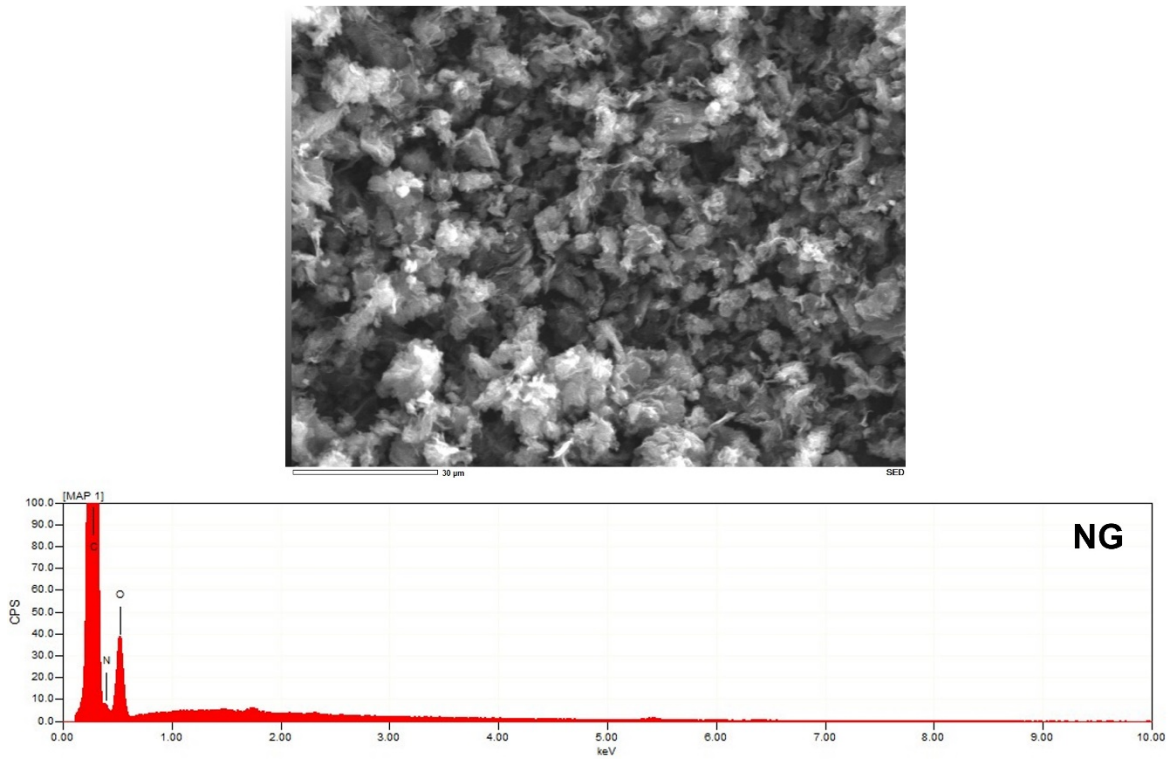

Fig. S17 Scanning electron microscopy (SEM) image of N-doped graphene at 1000-fold magnification and energy dispersive X-ray spectrum (EDS) of NG.

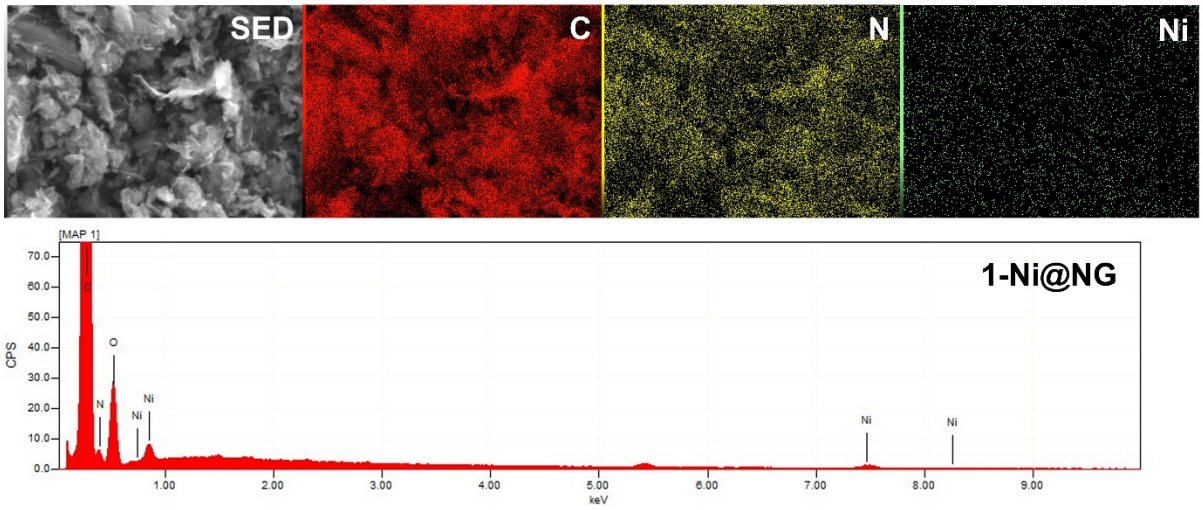

Fig. S18 3000-fold-magnified SEM images coupled with elemental mapping of **1-Ni@NG**. C (red), N (yellow), Ni (green). EDS spectrum of **1-Ni@NG**.

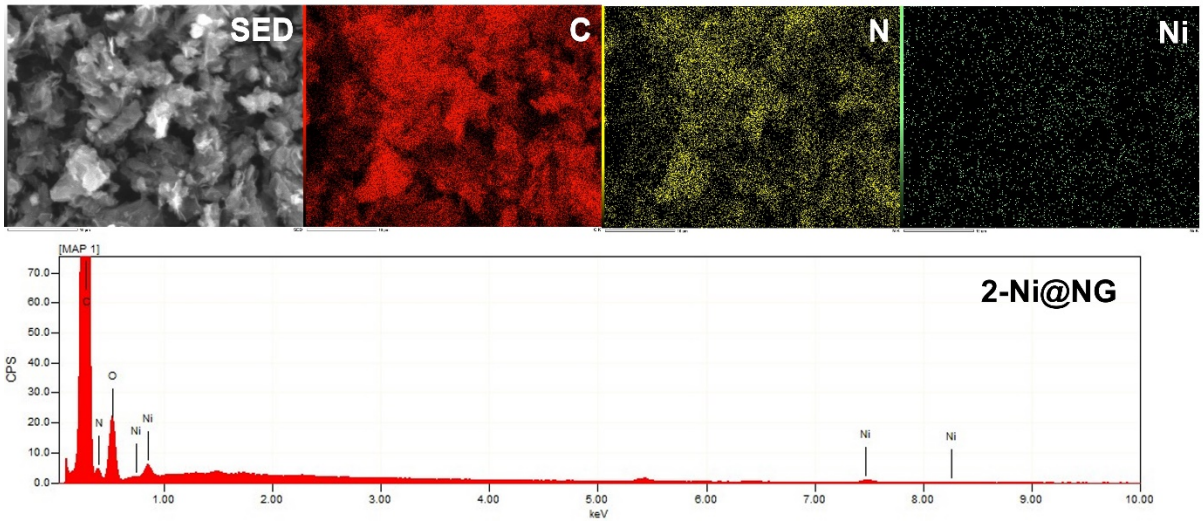

Fig. S19 3000-fold-magnified SEM images coupled with elemental mapping of **2-Ni@NG**. C (red), N (yellow), Ni (green). EDS spectrum of **2-Ni@NG.**

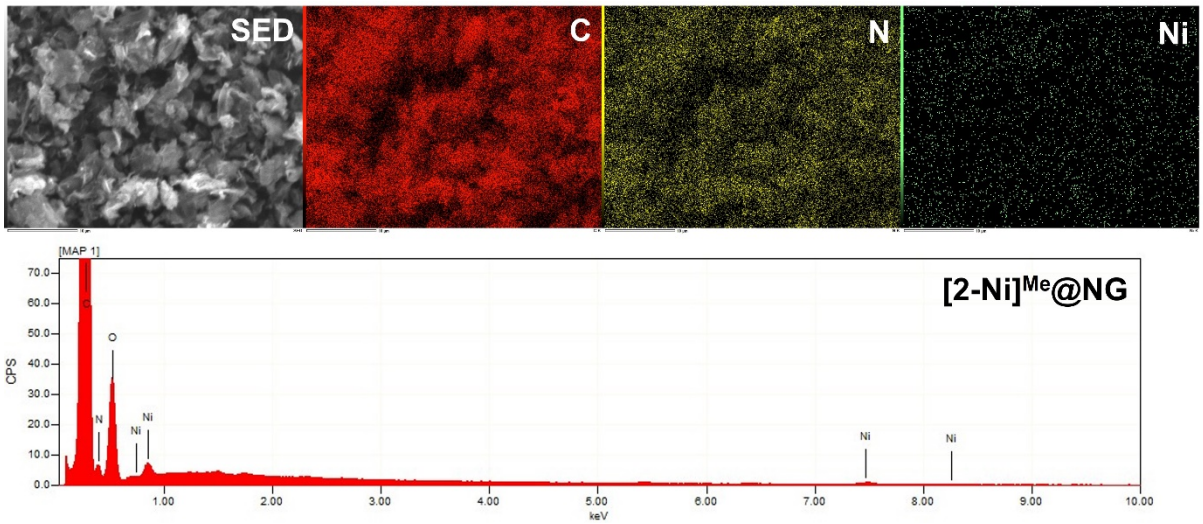

Fig. S20 3000-fold-magnified SEM images coupled with elemental mapping of **[2-Ni]^{Me}@NG**. C (red), N (yellow), Ni (green). EDS spectrum of **[2-Ni]^{Me}@NG**.

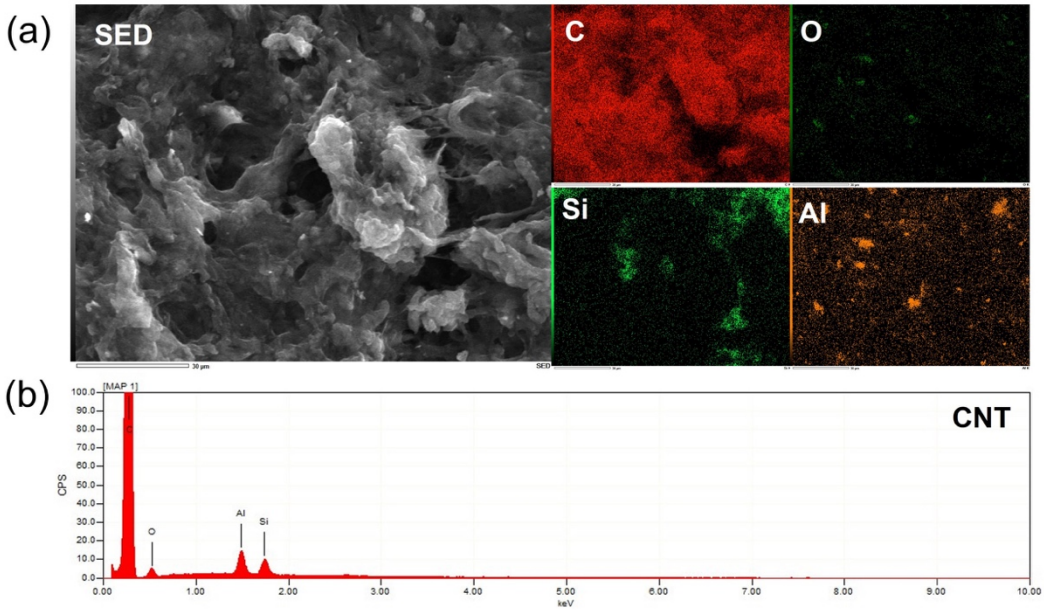

Fig. S21 (a) Scanning electron microscopic (SEM) image of pristine CNT and elemental mapping (C = red, O = dark green, Si = light green, Al = orange). (b) Energy dispersive X-ray spectroscopy (EDS) of pristine CNT. Silicon wafer was used as a holder for sample preparation.

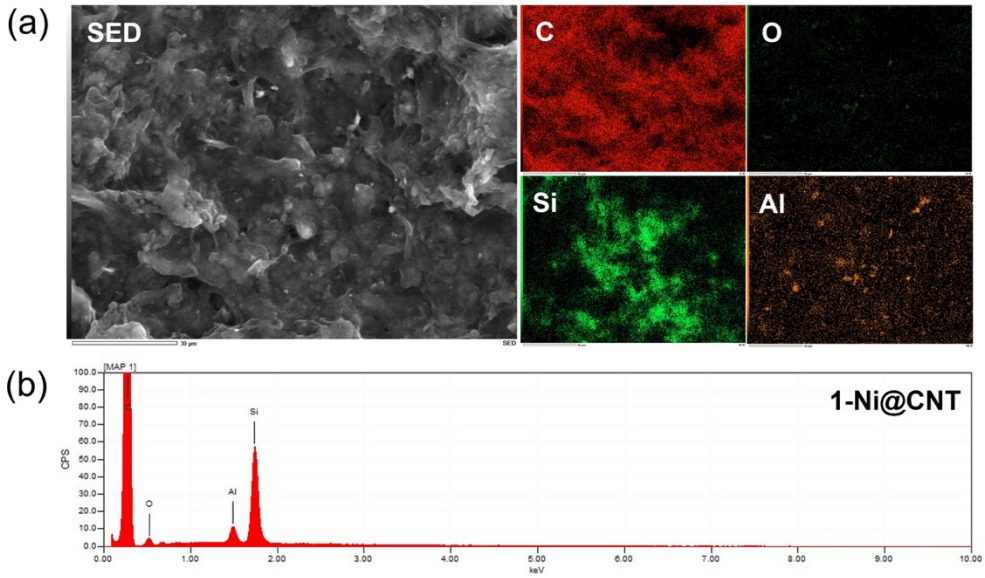

Fig. S22 (a) Scanning electron microscopic (SEM) image of **1-Ni@CNT** and elemental mapping (C = red, O = dark green, Si = light green, Al = orange). (b) Energy dispersive X-ray spectroscopy (EDS) of **1-Ni@CNT**. Silicon wafer was used as a holder for sample preparation.

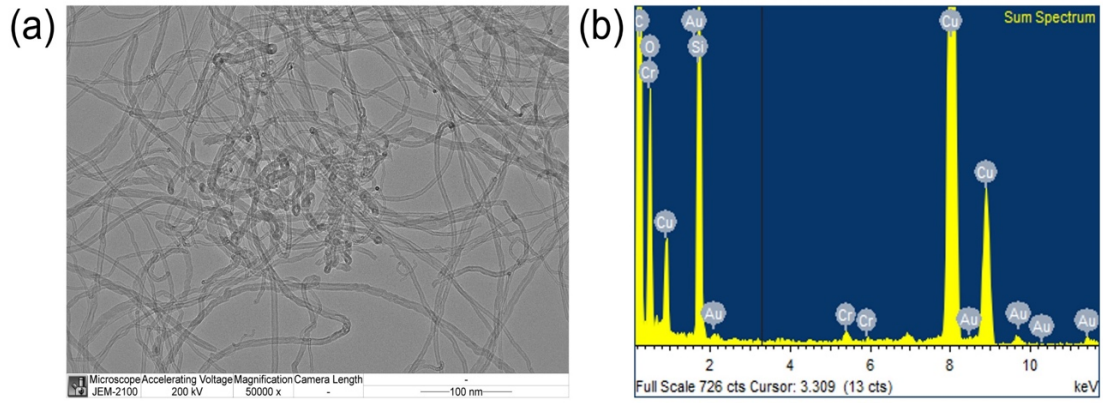

Fig. S23 (a) Transmission electron microscopic (TEM) image of **1-Ni@CNT**. (b) Energy dispersive X-ray spectroscopy (EDS) of **1-Ni@CNT**. Cu grid was used as a holder for sample preparation.

Electrochemical Studies in Aqueous Electrolyte

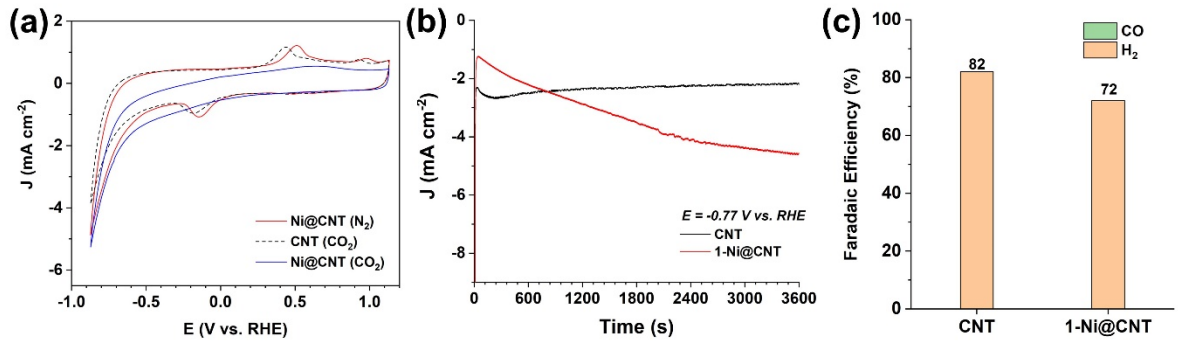

Fig. S24 (a) Cyclic voltammograms of CNT and **1-Ni@CNT** in 0.5 M $NaHCO_3$. (b) Chronoamperometric measurement of CNT and **1-Ni@CNT** in CO_2-saturated 0.5 M $NaHCO_3$ (pH = 7.3) for 1 h. (c) Faradaic efficiency of CNT and **1-Ni@CNT** showing only H_2 was observed during the bulk electrolysis.

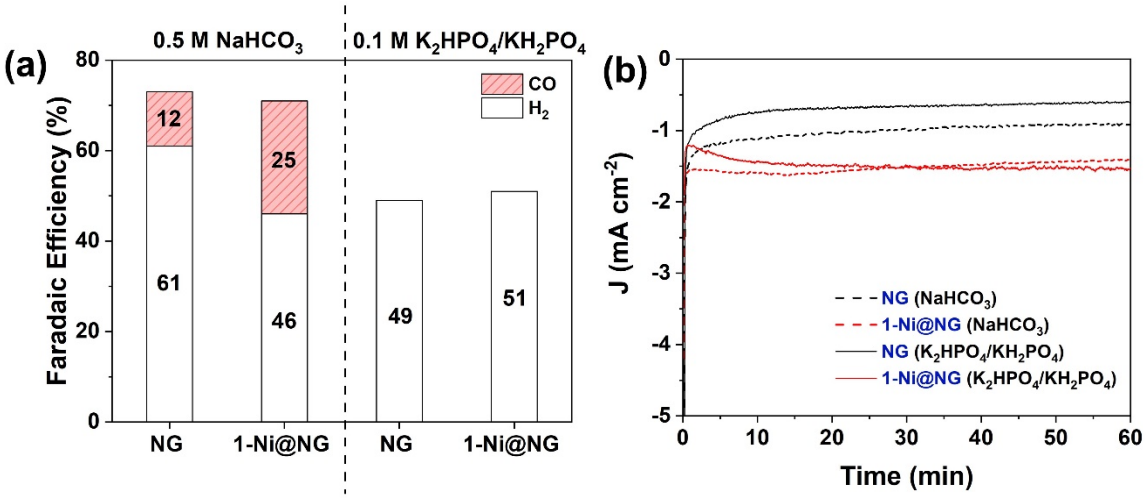

Fig. S25 (a) Faradaic efficiencies and (b) current-time profiles for 1 h-controlled potential electrolysis at -0.67 V *vs.* RHE in N_2-saturated 0.1 M K_2HPO_4/KH_2PO_4 (pH 8.1) of NG (black solid line) and **1-Ni@NG** (red solid line) versus in N_2-saturated 0.5 M $NaHCO_3$ (pH 8.7) of **NG** (black dotted line) and **1-Ni@NG** (red dotted line).

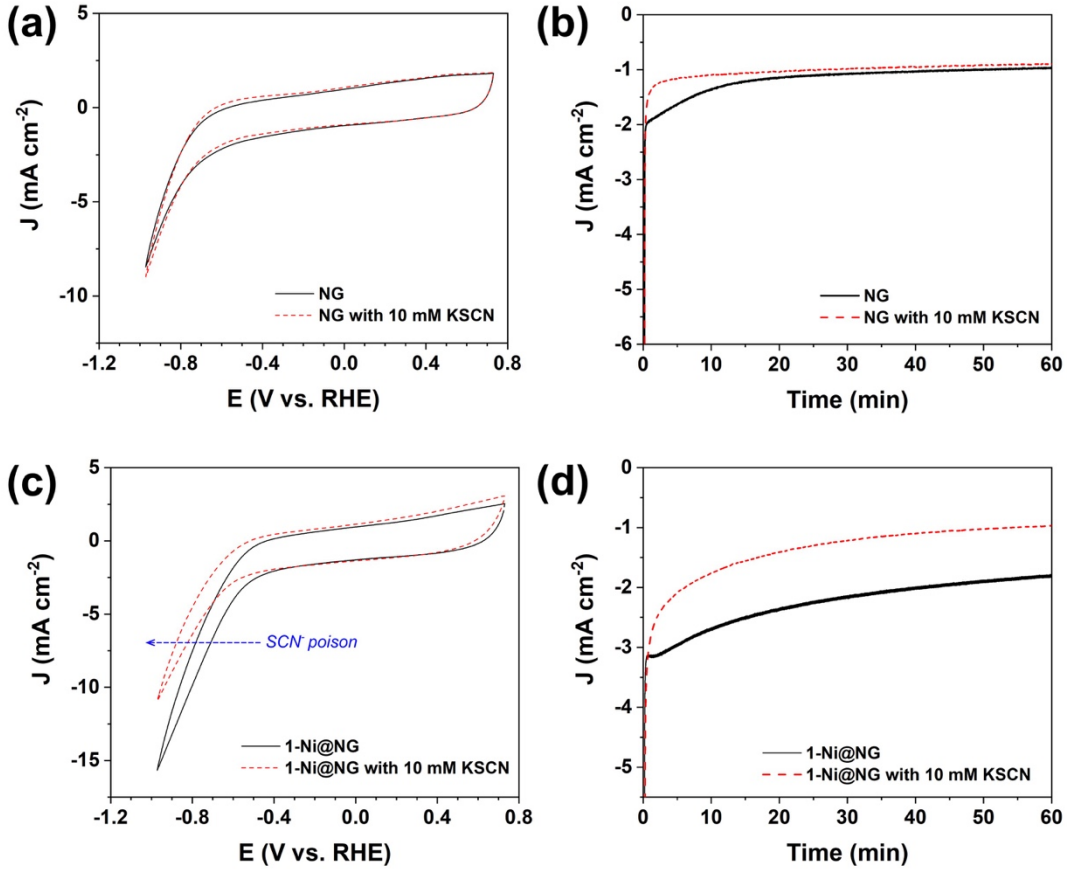

Fig. S26 KSCN poisoning test. (a) and (c) Cyclic voltammograms of NG and **1-Ni@NG** with and without 10 mM KSCN in 0.5 M $NaHCO_3$. (b) and (d) Current-time profiles of **NG** and **1-Ni@NG** with (red trace) and without (black trace) 10 mM KSCN in 0.5 M $NaHCO_3$.

Table S8 Electrochemical CO_2 reduction in the presence and absence of 10 mM KSCN at -0.67 V vs. RHE for 1 h

Catalysts	[KSCN]	Average Current Density (mA cm^{-2})	%FE(CO)	CO (μmol)
NG	0 mM	1.1	22	4.5
	10 mM	1.0	21	4.1
1-Ni@NG	0 mM	2.2	81	37.8
	10 mM	1.4	68	17.6

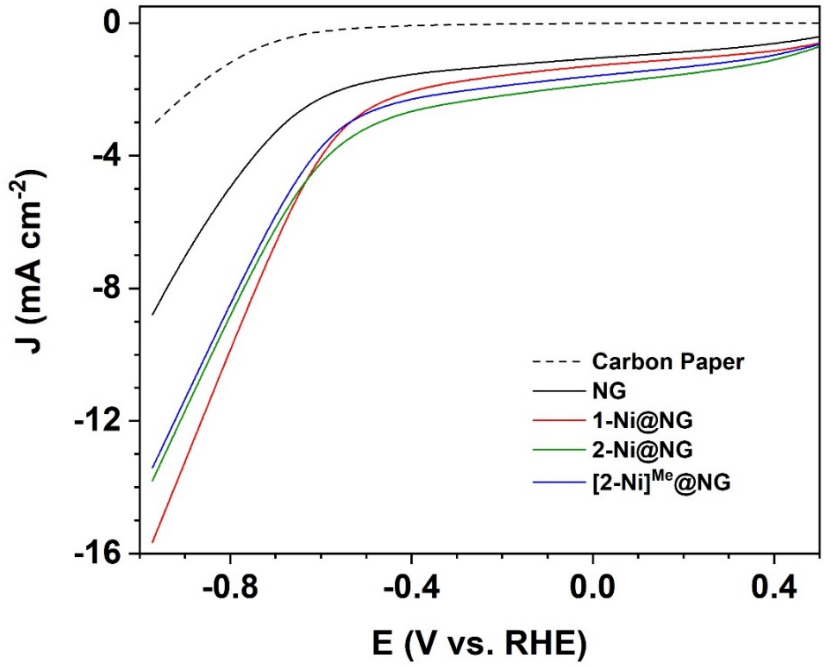

Fig. S27 Linear sweep voltammetry (LSV) in CO_2-saturated 0.5 M $NaHCO_3$ for carbon paper (black dotted line), NG (black solid line), **1-Ni@NG** (red solid line), **2-Ni@NG** (green solid line), and **[2-Ni]^{Me}@NG** (blue solid line) at the scan rate of 0.05 V/s.

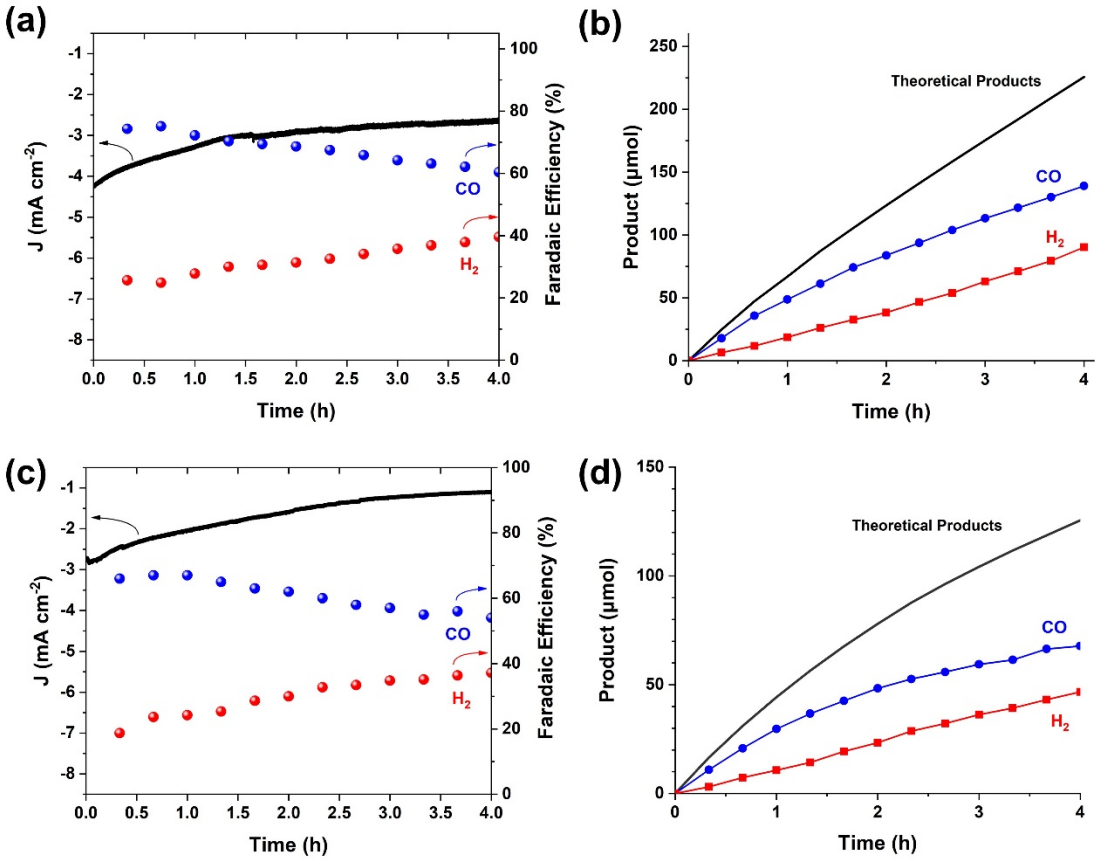

Fig. S28 Current-density time profiles and faradaic efficiencies of CO (blue) and H_2 (red) evolution in controlled potential electrolysis at -0.67 V *vs.* RHE (η = 0.56 V) in CO_2-saturated 0.5 M $NaHCO_3$ using (a)**2-Ni@NG** and (b) **[2-Ni]^{Me}@NG**. Time courses of the moles of CO (blue) and H_2 (red) production from bulk electrolysis and theoretical product yields (black) calculated from $e^-/2$ of charge required during the bulk electrolysis for (c) **2-Ni@NG** and (d) **[2-Ni]^{Me}@NG.**

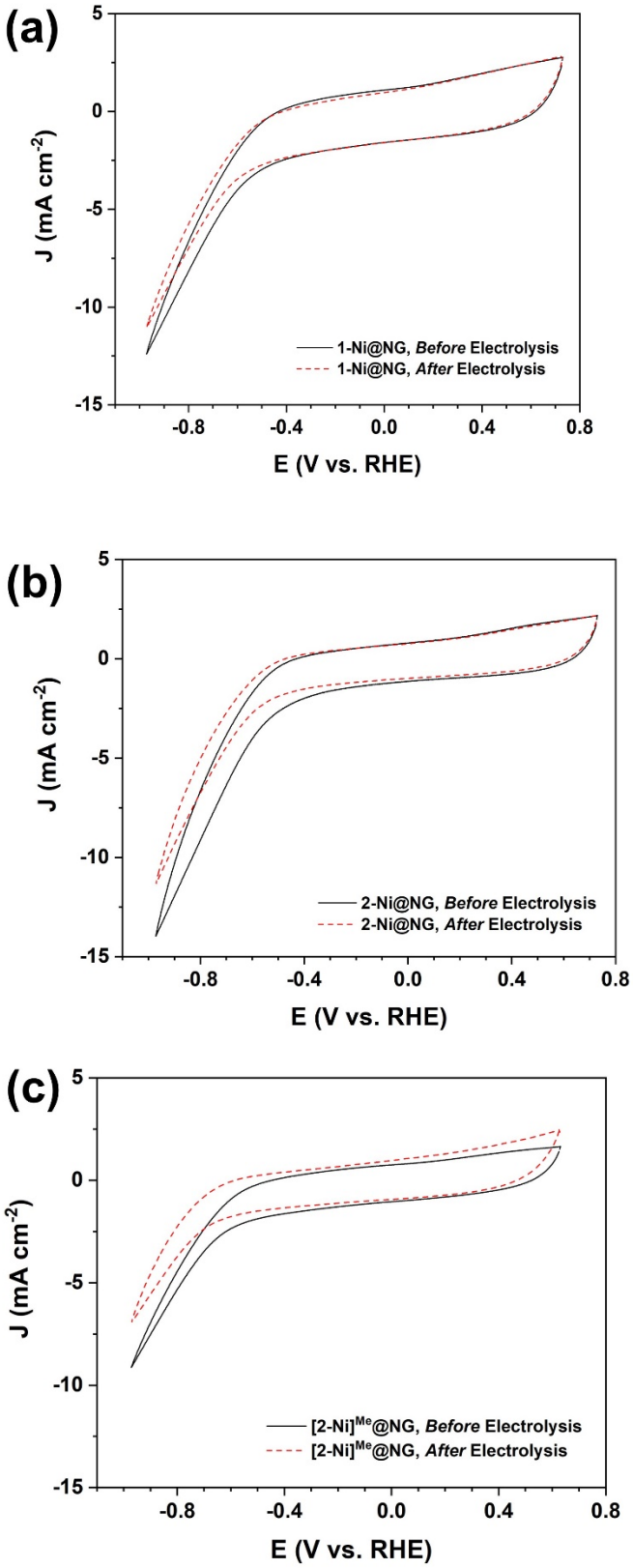

Fig. S29 Cyclic voltammetry in CO_2-saturated 0.5 M $NaHCO_3$ before (black solid line) and after electrolysis (red-dotted line) at -0.67 V vs. RHE for 4 h for (a) **1-Ni@NG**, (b) **2-Ni@NG** and (c) **[2-Ni]^{Me}@NG.**

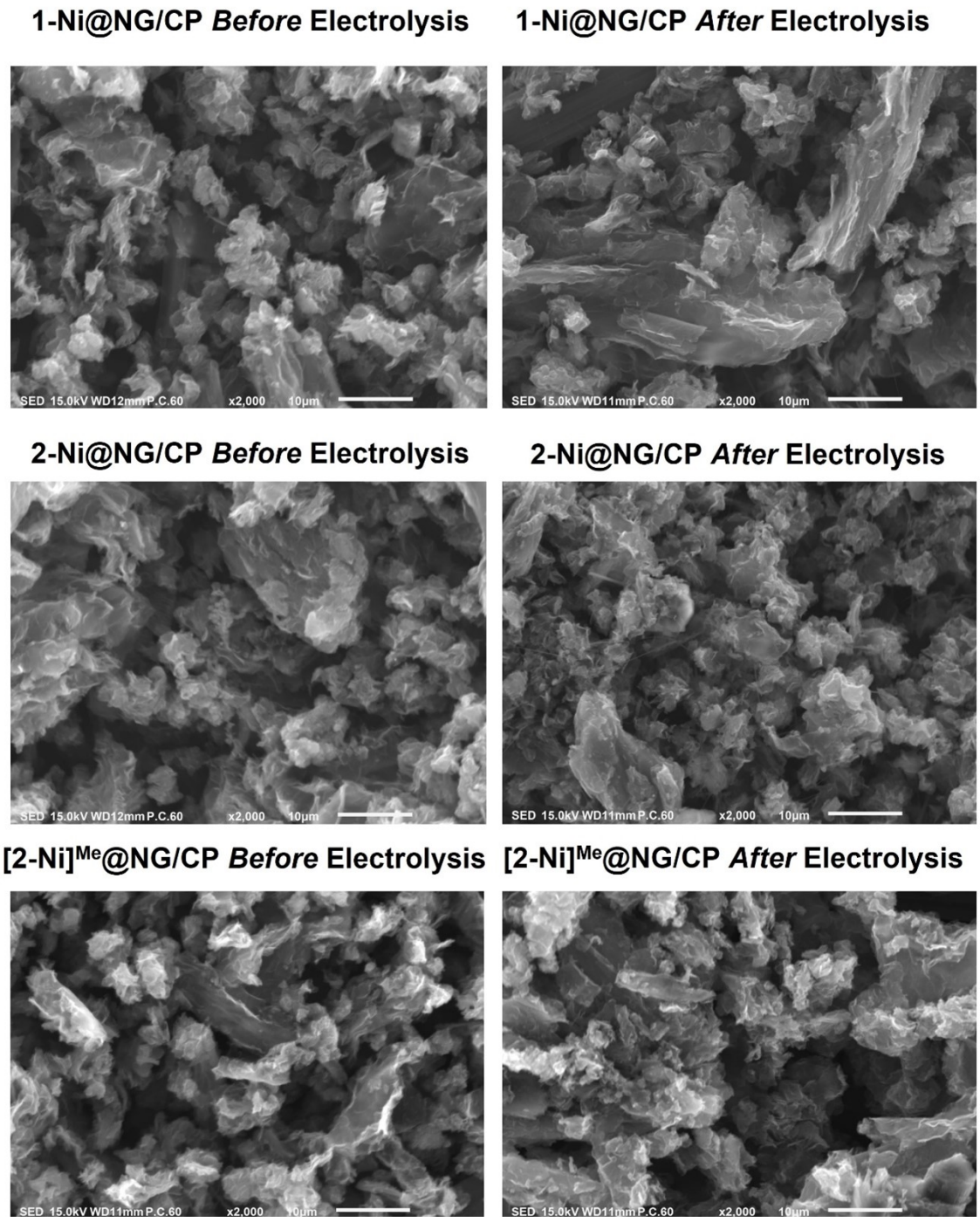

Fig. S30 SEM images at 2000-fold magnification of **1-Ni@NG/CP**, **2-Ni@NG/CP** and **[2-Ni]^{Me}@NG/CP** before and after electrocatalysis for 4 h at the applied potential of -0.67 V *vs.* RHE.

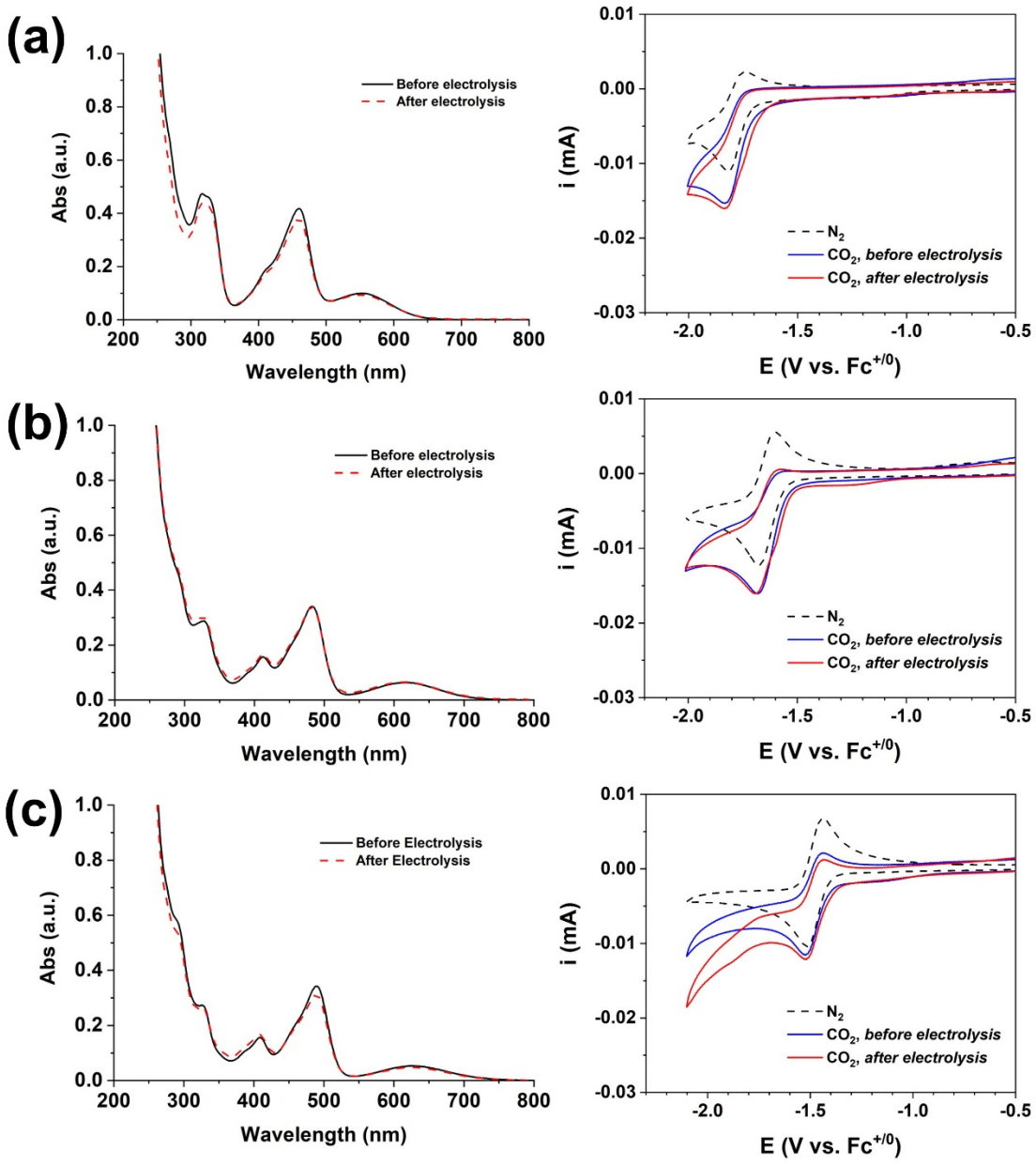

Fig. S31 UV-visible spectroscopy (left panel) and cyclic voltammograms (right panel) of (a) 1-Ni, (b) 2-Ni and (c) 2-Ni^{Me} before and after electrolysis at E = -1.85, -1.75 and -1.65 V vs. $Fc^{+/0}$ in CO_2-saturated 0.1 M N_4BuPF_6/CH_3CN.

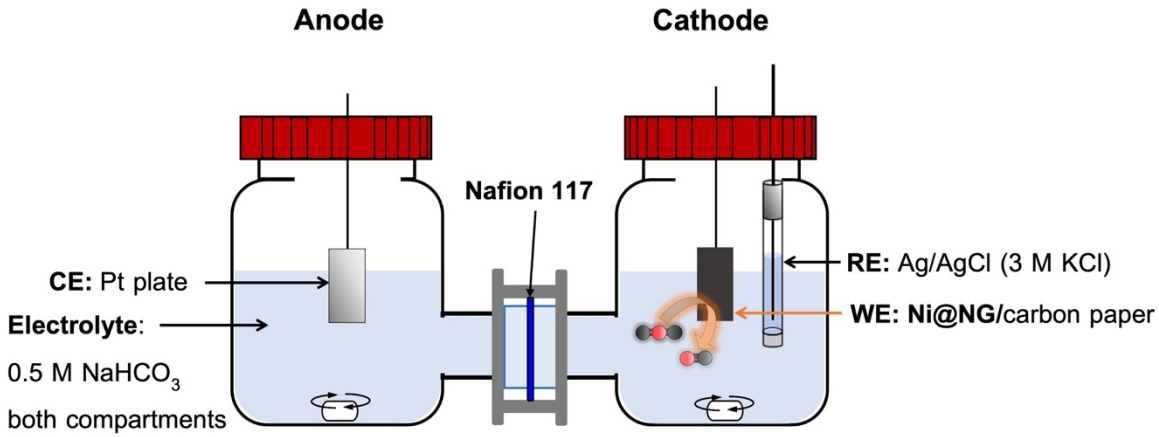

Fig. S32 A two-compartment three-electrode electrochemical setup for aqueous system.

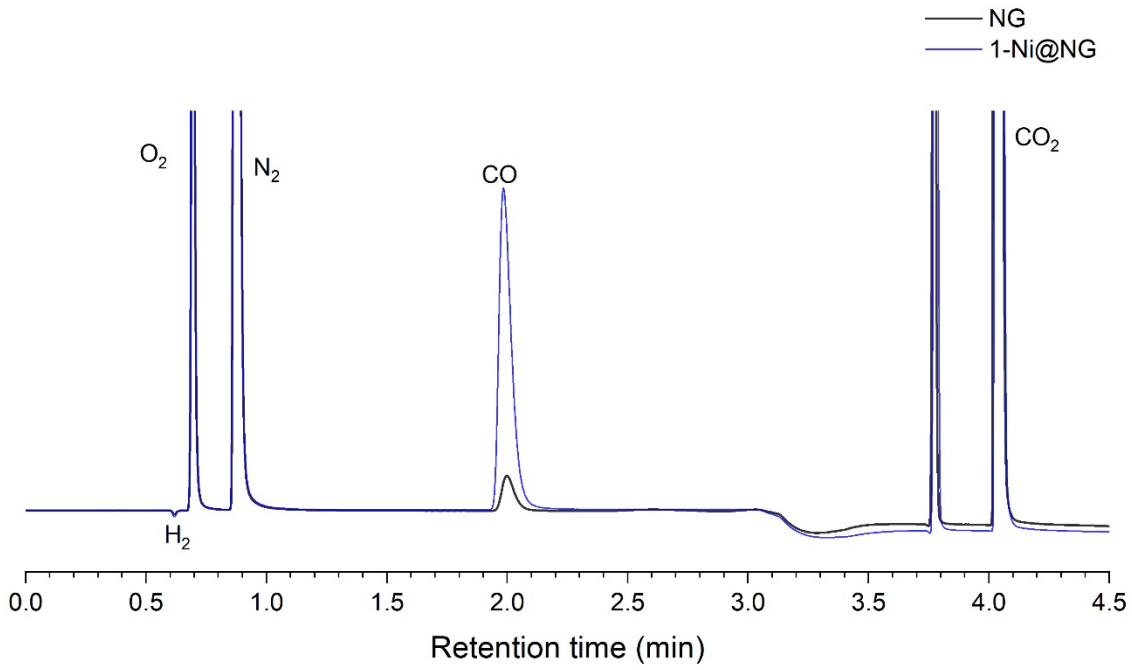

Fig. S33 GC traces of bulk electrolysis using NG (black) and 1-Ni@NG (blue) in 0.5 M $NaHCO_3$ at E = -0.77 V *vs.* RHE for 1 h. Retention time of H_2 (0.617), O_2 (0.694), N_2 (0.869), CO (2.010) and CO_2 (4.023). The carrier gas was He and the detector was a thermal conductivity detector (TCD).

Calculation of Faradaic Efficiency

$$\textbf{\%Faradaic Efficiency} = \frac{Q_{output}}{Q_{input}} \textbf{ x 100}$$

where e_{input} = the total number of moles of electrons measured during electrolysis

e_{output} = the number of moles of electrons required for reducing CO_2 to CO

For bulk electrolysis at *E = -0.77 V vs. RHE*

$e_{input} = \frac{Q}{F} = \frac{\int i\,dt}{F} = \frac{11.60\ C}{96485 \frac{C}{mole\ of\ electrons}}$ = 1.20 x 10^{-4} mole of electrons

Calculation of Faradaic Efficiency of CO

Volume of measured CO from GC = 4.42%, which was calibrated from standard gas

Head space of H-type cell = 28 mL

Hence, volume of CO produced = 28 mL x 0.0442 = 1.24 mL

Conversion of volume to mole of produced CO

From the law of ideal gases, PV = nRT

n = PV/RT

n = (1 atm)(1.24 x 10^{-3} L)/(0.0821 L atm mol^{-1} K^{-1})(298.15 K)

Thus, moles of produced CO n_{CO} = 5.07 x 10^{-5} mol

Electrochemical CO_2-to-CO conversion: $\mathbf{CO_2 + 2H^+ + 2e^- \rightarrow CO + H_2O}$

e_{output} = 5.07 x 10^{-5} mol of CO x $\frac{2\ mol\ of\ electrons}{1\ mol\ of\ CO}$ = 1.01 x 10^{-4} mol of electrons

Hence, %Faradaic Efficiency of CO = $\frac{e_{output}}{e_{input}}$ x 100 = $\frac{1.01 \times 10^{-4}\ mol\ of\ electrons}{1.20 \times 10^{-4}\ mol\ of\ electrons}$ x 100 = 84.2%

Calculation of Faradaic Efficiency of H_2

Volume of measured H_2 from GC = 0.87%, which was calibrated from standard gas

Head space of H-type cell = 28 mL

Hence, volume of produced H_2 = 28 mL x 0.0087 = 0.24 mL

Conversion of volume to mole of produced H_2

From the law of ideal gases, $PV = nRT$

$n = PV/RT$

$n = (1\ atm)(0.24 \times 10^{-3}\ L)/(0.0821\ L\ atm\ mol^{-1}\ K^{-1})(298.15\ K)$

Thus, moles of produced H_2 $n_{H2} = \underline{0.98 \times 10^{-5}}$ mol

Hydrogen Evolution Reaction (HER): $\mathbf{2H^+ + 2e^- \rightarrow H_2}$

e_{output} = 0.98 x 10^{-5} mol of H_2 x $\frac{2\ mol\ of\ electrons}{1\ mol\ of\ CO}$ = 1.96 x 10^{-5} mol of electrons

Hence, %Faradaic Efficiency of H_2 = $\frac{e_{output}}{e_{input}}$ x 100 = $\frac{1.96 \times 10^{-5}\ mol\ of\ electrons}{1.20 \times 10^{-4}\ mol\ of\ electrons}$ x 100 = 16.3%

Summarized Data of Bulk Electrolysis at Various Potential Applied

Table S9 Summary of data in bulk electrolysis in a CO_2-saturated 0.5 M $NaHCO_3$ solution (pH 7.4) using **1-Ni@NG**

$E_{applied}$ (V vs. RHE)	Time (h)	Charge (C)	CO (μmol)	%FE(CO)	H_2 (μmol)	%FE(H_2)
-0.57	1	3.4	11.0	62	5.9	33
-0.67	1	8.8	37.8	81	7.2	16
-0.77	1	11.6	50.7	84	9.8	16
-0.87	1	14.5	53.4	71	18.9	25

Table S10 Summary of data in bulk electrolysis in a CO_2-saturated 0.5 M $NaHCO_3$ solution (pH 7.4) using **2-Ni@NG**

$E_{applied}$ (V vs. RHE)	Time (h)	Charge (C)	CO (μmol)	%FE(CO)	H_2 (μmol)	%FE(H_2)
-0.57	1	3.3	10.7	63	6.1	36
-0.67	1	10.3	40.6	76	13.7	25
-0.77	1	14.7	58.6	77	35.0	23
-0.87	1	24.0	77.3	62	44.1	36

Table S11 Summary of data in bulk electrolysis in a CO_2-saturated 0.5 M $NaHCO_3$ solution (pH 7.4) using **[2-Ni]^{Me}@NG**

$E_{applied}$ (V vs. RHE)	Time (h)	Charge (C)	CO (μmol)	%FE(CO)	H_2 (μmol)	%FE(H_2)
-0.57	1	2.0	6.2	58	2.6	25
-0.67	1	5.6	19.2	68	4.9	17
-0.77	1	8.6	29.8	67	9.0	20
-0.87	1	14.1	56.3	77	11.8	16

Table S12 Comparison of selected bond lengths (Å), angles (°) and twist of diphenylamine unit for **1-Ni**, **2-Ni** and [**2-Ni**]^{Me}.

	1-Ni[a]	**2-Ni**[b]	[**2-Ni**]^{Me}
Bond lengths [Å]			
Ni1−N1	1.869(3)	1.867(2)	1.907(5)
Ni1−N2	1.861(7)	1.894(2)	1.914(4)
Ni1−N3	1.924(4)	1.942(2)	2.115(2)
Ni1−N4	1.830(7)	1.899(2)	2.014(4)
Bond angles [°]			
N1−Ni1−N2	94.9(3)	89.48(10)	87.4(2)
N1−Ni1−N3	179.3(4)	174.78(10)	175.12(2)
N1−Ni1−N4	95.3(3)	90.51(10)	92.0(2)
N2−Ni1−N3	85.2(3)	85.98(10)	88.34(2)
N2−Ni1−N4	169.83(19)	174.32(9)	179.5(2)
N3−Ni1−N4	84.6(3)	94.26(10)	92.2(2)
Twist of phenyl rings [°]	47.3	63.4	60.9

[a,b]Crystallographic data was obtained from ref. [S1] and [S2], respectively.

Table S13 Comparison of the ECR performance of Ni@NG catalysts from this work with high-performance ECR molecular-based catalysts from recent literatures.

Catalyst	Cathode Material	Electrolyte	Applied Potential (V vs. RHE)	J (mA/cm^2)	Product(s)	%FE	TOF (h^{-1})	Method for analyzing active surface area of catalyst	Ref
1-Ni@NG	Carbon Paper	0.5 M $NaHCO_3$ (pH 7.4)	-0.67	~2	CO	81	97.2	ICP-AES	This work
2-Ni@NG				~3		75	151.2		
$[2\text{-Ni}]^{Me}$@NG				~1.5		68	93.6		
Pyrene-modified Ni(cyclam)/MWCNT	GDL	0.1 M Bu_4NPF_6/ CH_3CN + 1% H_2O	-2.54[a]	~10	CO	>90	4.27(s^{-1})	ECSA	S3
NiPc	CFP	0.5 M $KHCO_3$ (pH 7.2)	-0.80	-	CO	<40	-	-	S4
NiPc/CNT	Carbon Paper	0.5 M $KHCO_3$ (pH 7.2)	-0.78	-	CO	78	1025	-	S5
PyNiPc/CNT				-		~100	8715	-	
Ni(Salen-NO_2)	GDL	0.5 M $KHCO_3$ (pH 7.5)	-1.50[b]	-	CO CH_4 C_2H_6	~40 ~17 ~17	-	-	S6
Ni(Salen-NH_2)/Graphite plates	Graphite Electrode	0.5 M $KHCO_3$ (pH 7.0)	-1.80[c]	-	HCOOH CH_3OH C_2H_5OH	4.7 11.4 28.6	0.33(s^{-1}) 0.8(s^{-1}) 2.1(s^{-1})	-	S7
Ni-CNT-PP	Glassy carbon, RDE	0.5 M $KHCO_3$ (pH 7.3)	-0.71	13.4	CO	96	0.6 x 10^5	ICP-OES	S8
Ni-CNT-CC				32.3	CO	99	~10^5		
Ni-PMOF	Carbon Cloth	0.5 M $KHCO_3$ (pH 7.2)	-0.80	0.47	CO	18.5	8.11	-	S9
Co-PMOF				~18	CO	98.7	1656		
CoPc	CFP	0.5 M $KHCO_3$ (pH 7.2)	-0.80	-	CO	99	~42	ECSA	S4
CoPc/CCG	Carbon paper	0.1 M $KHCO_3$ (pH 6.8)	-0.59	~0.8	CO	63	~2 (s^{-1})	ECSA	S10
CoPc-Py/CNT	Carbon paper	0.2 M $KHCO_3$ (pH 7.0)	-0.63	~5	CO	98	34.5(s^{-1})	Total Catalyst Loading	S11
CoFPc/carbon cloth	Carbon cloth	0.5 M $NaHCO_3$ (pH 7.3)	-0.80	~4	CO	93	1.6(s^{-1})	ICP-OES	S12
Fe(bpc)Cl(H_2O)/NG	GC	0.5 M $NaHCO_3$ (pH 7.3)	-0.58	~6	CO	90	2.1(s^{-1})	ECSA	S13
Fe-TPPy/CNT	GC	0.1 M $NaHCO_3$ (pH 6.8)	-0.60	19.6	CO CH_4	37 17	0.97(s^{-1}) 0.07(s^{-1})	-	S14
Fe-*adj*-TPPy/CNT	GC		-0.60	30.4	CO CH_4	67 25	3.49 (s^{-1}) 0.07(s^{-1})	-	

[a] Applied potential was reported in *V vs. $Fc^{+/0}$*, [b] Applied potential was reported in *V vs. SHE*, [c] Applied potential was reported in *V vs. Ag/AgCl,* ECSA = electrochemically active surface area, CFP = carbon fibre paper, GDL = gas diffusion electrode, GC = glassy carbon, RDE = rotating disk electrode, Pc = phthalocyanine, bpc = 4,5-dichloro-1,2-bis(pyridine-2-carboximido)benzene, CCG = chemically converted graphene, CNT = carbon nanotube, MWCNT = multi-walled carbon nanotube.

References

[S1] R. Sanyal, S. A. Cameron and S. Brooker, *Dalton Trans.* **2011**, *40*, 12277-12287.

[S2] R. K. Wilson and S. Brooker, *Dalton Trans.* **2013**, *42*, 7913-7923.

[S3] S. Pugliese, N. T. Huan, J. Forte, D. Grammatico, S. Zanna, B. L. Su, Y. Li and M. Fontecave, *ChemSusChem*, **2020**, 13, 6449-6456.

[S4] Z. Zhang, J. Xiao, X. J. Chen, S. Yu, L. Yu, R. Si, Y. Wang, S. Wang, X. Meng, Y. Wang, Z. Q. Tian and D. Deng, *Angew. Chem. Int. Ed*., **2018**, 57, 16339-16342.

[S5] D.-D. Ma, S.-G. Han, C. Cao, X. Li, X.-T. Wu and Q.-L. Zhu, *Appl. Catal. B*, **2020**, 264.

[S6] S. Singh, B. Phukan, C. Mukherjee and A. Verma, *RSC Adv.*, **2015**, 5, 3581-3589.

[S7] P. Bose, C. Mukherjee and A. K. Golder, *Inorg. Chem. Front.*, **2019**, 6, 1721-1728.

[S8] S. Liu, H. B. Yang, S. F. Hung, J. Ding, W. Cai, L. Liu, J. Gao, X. Li, X. Ren, Z. Kuang, Y. Huang, T. Zhang and B. Liu, *Angew. Chem. Int. Ed.*, **2020**, 59, 798-803.

[S9] Y. R. Wang, Q. Huang, C. T. He, Y. Chen, J. Liu, F. C. Shen and Y. Q. Lan, *Nat. Commun.*, **2018**, 9, 4466.

[S10] J. Choi, P. Wagner, S. Gambhir, R. Jalili, D. R. MacFarlane, G. G. Wallace and D. L. Officer, *ACS Energy Lett.*, **2019**, 4, 666-672.

[S11] M. Zhu, J. Chen, R. Guo, J. Xu, X. Fang and Y.-F. Han, *Appl. Catal. B*, **2019**, 251, 112-118.

[S12] N. Morlanés, K. Takanabe and V. Rodionov, *ACS Catal.*, **2016**, 6, 3092-3095.

[S13] E. A. Mohamed, Z. N. Zahran, Y. Tsubonouchi, K. Saito, T. Yui and M. Yagi, *ACS Appl. Energy Mater.*, **2020**, 3, 4114-4120.

[S14] M. Abdinejad, C. Dao, B. Deng, F. Dinic, O. Voznyy, X.-a. Zhang and H.-B. Kraatz, *ACS Sustain. Chem. Eng.*, **2020**, 8, 9549-9557.